On the superluminal propagation of X-shaped localized waves

2000 J. Phys. A: Math. Gen. 33 7227

(http://iopscience.iop.org/0305-4470/33/40/317)

J. Phys. A: Math. Gen. **33** (2000) 7227–7254. Printed in the UK PII: S0305-4470(00)13288-3

On the superluminal propagation of X-shaped localized waves

Amr M Shaarawi†§ and Ioannis M Besieris‡

† School of Science and Engineering, American University in Cairo, PO Box 2511, Cairo 11511, Egypt

‡ Bradley Department of Electrical and Computer Engineering, Virginia Polytechnic Institute and State University, Blacksburg, VA 24061, USA

Received 13 April 2000, in final form 20 July 2000

Abstract. The generation and propagation of superluminal X-shaped pulses is investigated. We demonstrate that such pulses can be modelled using a spectral approach that produces time-limited Bessel beams. Special attention is given to calculating the velocities of the modelled pulsed Bessel beams. The velocities of the peaks of the resulting pulses depend on the shapes of the spatio-temporal distributions of the applied time-windows. The generation of pulsed Bessel beams is investigated for various set-ups; including circular arrays, annular slits and axicons. It is shown that superluminal pulsed Bessel beams undergo a delayed generation before they are launched; henceforth, the peak of these pulses travels at speeds exceeding that of light.

1. Introduction

In recent years, several pulsed wave solutions that have peaks travelling at superluminal speeds have been introduced. Examples of such solutions are the X-wave [1, 2], the Bessel X-pulse [3–5] and the focused X-wave [6]. There have been suggestions that the existence of such pulsed solutions may contradict the theory of special relativity [7–10]. Moreover, claims have been made that the existence of such signals implies 'a breakdown of the principle of relativity' [10]. The aim of this work is to study the details of the generation of such pulsed fields and to discuss their implication as far as special relativity is concerned.

All X-shaped superluminal solutions [1–6, 11–16] appearing in literature can be synthesized as superpositions of Durnin's Bessel beam solution [17–19]. The azimuthally symmetric zero-order Bessel beam is given by

$$\Psi(\vec{r}, t) = J_0(\chi\rho)\mathrm{e}^{-\mathrm{i}(k_z z - \omega_0 t)} \tag{1}$$

where $\omega_0^2 = \chi^2 + k_z^2$. The exact Bessel beams do not diffract because they require infinite apertures to excite them. In practical situations, approximate Bessel beams are generated using finite-size sources obtained by truncating the Bessel profile of the initial excitation of the source [19–23]. Such approximate Bessel beams have finite diffraction-free ranges, beyond which they spread out.

The first optical Bessel beam was generated by Durnin *et al* via the illumination of an annular slit placed in the focal plane of a lens [19]. Durnin demonstrated that a finite Bessel beam had a larger field depth compared with a Gaussian beam, even if their central spots had equal radii. Other methods have been suggested to generate optical and acoustical

§ Permanent address: Department of Engineering Physics and Mathematics, Faculty of Engineering, Cairo University, Giza 12211, Egypt.

0305-4470/00/407227+28$30.00

Bessel beams. One of the methods for generating optical Bessel beams utilizes a point source illumination of a Fabry–Perot interferometer [24, 25]. The aperture of a lens placed behind the interferometer is adjusted so that it transmits only the first ring and blocks all other rings. Consequently, the transmitted image becomes that of a zero-order Bessel function. In addition, conical lenses (axicons) have been used to generate a superposition of equally weighted monochromatic plane waves lying on a conical surface characterizing the spectral structures of the generated Bessel beams [23, 26, 27]. Other groups have employed holographic optical elements that introduce phase factors analogous to the linear phase delays contributed by refractive axicons [28–33]. Beside the aforementioned optical schemes, there have been successful designs of acoustical Bessel beam sources. The first acoustical Bessel beam generator was reported by Hsu *et al* [34]. They constructed a three-ring narrow-band solid PZT transducer. Applying Bessel shading Hsu *et al* used such a transducer to generate a continuous-wave Bessel beam. A second acoustical source was developed by Lu and Greenleaf who used an improved acoustical transducer [35, 36]. They constructed a wideband ten-ring annular transducer from a PZT ceramic/polymer composite. The same source has been used to generate ultrasonic monochromatic Bessel beams, as well as pulsed fields such as the X-wave [2]. The latter is a broadband pulse generated when the excitation of each array element has an independent temporal profile. The source built by Lu and Greenleaf has been used to investigate the application of ultrasonic Bessel beams and X-waves in medicine; e.g. high-resolution imaging [35–40] and using the Doppler effect for estimating the velocity of blood flow [41].

Studies of ultra-wideband localized wave (LW) solutions to the homogenous wave equation have developed in parallel to investigations of Durnin's monochromatic Bessel beams. Examples of the former include the focus wave modes [42–45], the modified power spectrum pulse [44–50], the X-wave [1, 2], the Bessel X-pulse [3–5] and the focus X-wave [6]. These LW solutions are superpositions of polychromatic Bessel beams. The time dependence of the initial excitations of the different sections of their sources is mirrored in their spatio-temporal Fourier spectra. LW pulses exhibit characteristic spatio-temporal spectral couplings that depend on the spatio-temporal distribution of their excitations [51–54]. Therefore, one may perceive LW fields as Bessel beams that are time-limited using intricate spatio-temporal windowing functions. Furthermore, the differences between various LW solutions might be attributed to the nature of the spatio-temporal windowing of Bessel beam sources. A monochromatic zero-order Bessel beam is a superposition of equally weighted monochromatic plane waves having propagation vectors lying on a conical surface [11, 12, 17–19]. On the other hand, a pulsed Bessel beam (or a LW pulse) has a large frequency bandwidth and both its temporal and spatial spectral components are designed to produce a highly directional time-limited pulse [51–54]. For example, the X-waves are weighted superpositions over polychromatic Bessel beams restricted to a single conical surface [12, 13]. On the other hand, the focus wave modes are composed of polychromatic Bessel beams acquiring different spectral amplitudes over an infinite number of uniaxial conical surfaces [55]. One should also note that not all LW pulses are superluminal. Only, LW solutions deduced using the superluminal boost superposition have peaks that propagate at superluminal velocities [6].

It is an established theoretical result that the velocity of the peak of an optical X-shaped LW (or a pulsed Bessel beam) can be superluminal [1–16]. Furthermore, it has been demonstrated experimentally that the peak of an *acoustic* X-wave generated using the circular array of Lu and Greenleaf travels at a supersonic speed [8]. Based on an extrapolation of the results of the acoustical experiment to the case of optical pulses, it has been argued that the generation of superluminal X-waves would entail a violation of the theory of special relativity [8]. This argument needs to be examined more carefully in view of the optical X-shaped localized

waves generated in an experiment performed by Saari and Reivelt [4] and the observation of the superluminal behaviour of microwave X-shaped LWs reported by Mugnai *et al* [56]. The main aim of this work is to investigate the prospect of superluminal signalling using pulsed Bessel beams. We provide a detailed analysis of the fields produced by different sources. The results of such calculations serve two goals. They provide preliminary estimates of what one should expect to observe in a real experiment. In addition, they clarify certain aspects related to the nature of the superluminal propagation of X-shaped localized pulses generated using various schemes.

The plan of this work is to investigate the various set-ups that can be used for generating pulsed Bessel beams. In section 2, we consider the case of pulsed Bessel beams generated from a circular aperture. In practical situations, the aperture would be built from discrete circular elements forming an array similar to the ultrasonic transducer built by Lu and Greenleaf. We demonstrate that the time-switching profile of the initial excitation of the aperture can affect the velocity of the peak of the generated pulses. From this analysis, we determine the conditions for producing either subluminal or superluminal pulsed Bessel beams. Generating pulsed Bessel beams using a uniform illumination of an annular slit is considered in section 3. In this case, we show that the superluminal speed of the peak of the pulsed Bessel beam is a consequence of a 'delayed generation' followed by a 'catching up' behaviour. In section 4, the case of generating a pulsed Bessel beam from an axicon is considered. In section 5, we provide our concluding remarks.

2. Pulsed Bessel beams generated by circular apertures

In this section, we investigate the case of pulsed Bessel beams generated from flat circular apertures. The analysis used here is based on a spectral synthesis of the driving function and is employed to highlight several essential features of pulsed Bessel beams. We introduce several spatio-temporal initial distributions of the driving functions of flat circular apertures. In practical situations, these initial distributions can be either time-limited, spatially shaded illuminations of the source plane, or initial current distributions driving an arrangement of discrete source elements. It should be noted that the first type has been the basis for recently reported optical and microwave sources [3–5, 56], while the second type has been used in generating acoustical pulsed Bessel beams [2, 44, 45]. An electromagnetic source of the second type, specifically a physical antenna driven by currents fed to its elements has not yet been realized. To set up a general framework to be used in later sections, we start by calculating the monochromatic Bessel beam radiated by an infinite source. This is followed by a discussion of using Fourier synthesis to time limit the initial excitation of a Bessel beam. We demonstrate that this can be done in diverse fashions and illustrate the differences among them. It will be shown that the way the initial Bessel beam excitation is time limited is crucial for determining the velocity of the peak of the generated pulse.

2.1. Monochromatic Bessel beams generated by an infinite source

A solution to the scalar wave equation can be written as a Fourier–Hankel superposition; specifically,

$$\Psi(\rho, z, t) = (1/2\pi) \int_{-\infty}^{+\infty} \mathrm{d}\omega \int_{0}^{\infty} \mathrm{d}\chi \; \chi J_0(\chi\rho) \mathrm{e}^{-\mathrm{i}z\sqrt{(\omega/c)^2-\chi^2}} \mathrm{e}^{\mathrm{i}\omega t} \Phi_{\mathrm{F}}(\chi, \omega). \tag{2}$$

Classes of wave solutions that are superpositions of Bessel beams are obtained by using the following spectrum:

$$\Phi_{\mathrm{F}}(\chi,\omega) = g(\chi,\omega)\delta(\chi - (\omega/c)\sin\xi). \tag{3}$$

The specific choice

$$g(\chi,\omega) = (2\pi/\chi)\delta(\omega-\omega_0) \tag{4}$$

yields the monochromatic Bessel beam solution [17]

$$\Psi(\vec{r},t) = J_0((\omega_0/c)\rho\sin\xi)\mathrm{e}^{-\mathrm{i}(\omega_0/c)(z\cos\xi - ct)}. \tag{5}$$

Here, the parameter ξ is the axicon angle. The above result is the same as that given in equation (1) after using the transformation $\chi = (\omega_0/c)\sin\xi$ and $k_z = (\omega_0/c)\cos\xi$. Note that the Bessel beam has a phase dependence that propagates at the superluminal speed $c/\cos\xi$. The representation given in equation (2) is a combination of monochromatic ($\omega = \omega_0$) plane waves propagating along tilted directions forming a circular conical surface defined by an apex angle ξ [12, 13, 17–19]. Other choices of $g(\chi,\omega)$ lead to a variety of LW fields [6, 48, 49, 54, 57].

Before examining the behaviour of pulsed Bessel beams radiated from finite apertures, we first demonstrate the invariance of the continuous Bessel beams radiated from planar sources having infinite extension. The field generated by an infinite source situated at the $z = 0$ plane is calculated using the Rayleigh–Sommerfeld formula [58]

$$\Psi(\rho,z,t) = (1/2\pi)\int_0^{2\pi}\mathrm{d}\phi'\int_0^{\infty}\mathrm{d}\rho'\rho'(1/R)\left\{[-\partial\Psi(\rho',z',t')/\partial z']_{z'=0}\right\}_{t'=t-R/c} \tag{6}$$

where $R = \sqrt{\rho'^2+\rho^2-2\rho\rho'\cos\phi'+z^2}$. The primed coordinates refer to points on the source plane and unprimed ones are related to observation points at $z > 0$. Assume that the initial excitation $\Psi(\rho',z'=0,t')$ is the Bessel beam given in equation (5), hence,

$$\Psi(\rho,z,t) = \frac{\mathrm{i}\omega_0}{2\pi c}\int_0^{2\pi}\mathrm{d}\phi'\int_0^{\infty}\mathrm{d}\rho'\,\rho'\cos\xi\,J_0((\omega_0/c)\rho'\sin\xi)\,\mathrm{e}^{\mathrm{i}\omega_0 t}\frac{\mathrm{e}^{-\mathrm{i}(\omega_0/c)R}}{R}. \tag{7}$$

To evaluate this integration, we use the formula

$$\frac{\mathrm{e}^{-\mathrm{i}(\omega_0/c)R}}{R} = \frac{1}{\pi}\int_0^{\infty}\mathrm{d}\lambda\,\lambda\int_{-\infty}^{+\infty}\mathrm{d}k_z\,J_0(\lambda\rho^*)\frac{\mathrm{e}^{-\mathrm{i}k_z z}}{k_z^2-((\omega_0/c)^2-\lambda^2)} \tag{8}$$

where $\rho^* = \sqrt{\rho^2+\rho'^2-2\rho\rho'\cos\phi'}$. From equations (7) and (8), we have

$$\begin{aligned}\Psi(\rho,z,t) = {}& \frac{\mathrm{i}\omega_0}{2\pi c}\int_0^{2\pi}\mathrm{d}\phi'\int_0^{\infty}\mathrm{d}\rho'\,\rho'\cos\xi\,J_0((\omega_0/c)\rho'\sin\xi)\\ &\times\mathrm{e}^{\mathrm{i}\omega_0 t}\frac{1}{\pi}\int_0^{\infty}\mathrm{d}\lambda\,\lambda\int_{-\infty}^{+\infty}\mathrm{d}k_z\,J_0(\lambda\rho^*)\frac{\mathrm{e}^{-\mathrm{i}k_z z}}{k_z^2-((\omega_0/c)^2-\lambda^2)}.\end{aligned} \tag{9}$$

Following the steps described in [14, 55], we can use the two identities

$$\int_0^{2\pi}\mathrm{d}\phi'\,J_0(\lambda\sqrt{\rho^2+\rho'^2-2\rho\rho'\cos\phi'^2}) = 2\pi\,J_0(\lambda\rho)J_0(\lambda\rho')$$

$$\frac{1}{\pi}\int_{-\infty}^{+\infty}\mathrm{d}k_z\,\frac{\mathrm{e}^{\mathrm{i}k_z z}}{k_z^2-((\omega_0/c)^2-\lambda^2)} = -\mathrm{i}\frac{\mathrm{e}^{-\mathrm{i}z\sqrt{(\omega_0/c)^2-\lambda^2}}}{\sqrt{(\omega_0/c)^2-\lambda^2}}$$

for $z \geqslant 0$, and the orthogonality of the Bessel functions [59] to obtain

$$\Psi(\rho, z, t) = J_0((\omega_0/c)\rho \sin\xi)\, \mathrm{e}^{\mathrm{i}\omega_0 t} \mathrm{e}^{-\mathrm{i}(\omega_0/c)\cos\xi z}.$$

This is the initial illumination used to excite the infinite aperture. As expected, an infinite aperture generates a non-diffracting Bessel beam.

For an initial excitation composed of a superposition of Bessel beams (cf equation (2)), the radiated field is also invariant with distance. Specifically, the field

$$\Psi(\rho, z, t) = (1/2\pi) \int_{-\infty}^{+\infty} \mathrm{d}\omega \int_0^{\infty} \mathrm{d}\chi\ \chi J_0(\chi\rho) \mathrm{e}^{-\mathrm{i}z\sqrt{(\omega/c)^2-\chi^2}} \mathrm{e}^{\mathrm{i}\omega t} \Phi_{\mathrm{F}}(\chi, \omega) \tag{10}$$

for $z > 0$, is diffraction free if generated from an infinite aperture. This well known result has been deduced previously using different methods [6, 12–16, 49, 55]. However, the derivation of this simple result has been repeated in this section because it provides the basis for a uniform approach to the modelling of time-limited Bessel beams.

2.2. Pulsed Bessel beams generated by finite-time sources

2.2.1. Spatially uniform Gaussian time window. A pulsed Bessel beam can be generated using different spatio-temporal excitation schemes. The simplest method is to time-window the initial beam excitation uniformly across an infinite source plane. In particular, we use a Gaussian window to time limit the initial field, namely,

$$\Psi_p(\rho, z = 0, t) = J_0((\omega_0/c)\sin\xi\rho)\, \mathrm{e}^{\mathrm{i}\omega_0 t} \mathrm{e}^{-t^2/4T^2}. \tag{11}$$

The spectrum corresponding to such an illumination wave field is calculated using a Hankel–Fourier transform; specifically,

$$\Phi_{\mathrm{F}}^{(1)}(\chi, \omega) = \int_0^{\infty} \mathrm{d}\rho\ \rho \int_{-\infty}^{+\infty} \mathrm{d}t\ J_0(\chi\rho) J_0((\omega_0/c)\sin\xi\rho)\, \mathrm{e}^{\mathrm{i}\omega_0 t} \mathrm{e}^{-t^2/4T^2} \mathrm{e}^{-\mathrm{i}\omega t}. \tag{12}$$

The integrations over ρ and t yield the following spectrum:

$$\Phi_{\mathrm{F}}^{(1)}(\chi, \omega) = \left(2T\sqrt{\pi}/\chi\right)\delta(\chi - (\omega_0/c)\sin\xi) \mathrm{e}^{-T^2(\omega-\omega_0)^2}. \tag{13}$$

Following the analysis presented in section 2.1 for an infinite aperture, the Rayleigh–Sommerfeld formula [58] gives the following polychromatic field:

$$\begin{aligned}\Psi_p(\rho, z, t) = (1/2\pi) &\int_{-\infty}^{+\infty} \mathrm{d}\omega \int_0^{\infty} \mathrm{d}\chi\ \chi J_0(x\rho) \mathrm{e}^{-\mathrm{i}z\sqrt{(\omega/c)^2-x^2}} \\ &\times \mathrm{e}^{\mathrm{i}\omega t}\left(2T\sqrt{\pi}/\chi\right)\delta(x - (\omega_0/c)\sin\xi) \mathrm{e}^{-T^2(\omega-\omega_0)^2}\end{aligned} \tag{14}$$

for $z > 0$. The integration over χ yields

$$\Psi_p(\rho, z, t) = \left(T/\sqrt{\pi}\right) \int_{-\infty}^{+\infty} \mathrm{d}\omega\ J_0((\omega_0/c)\rho\sin\xi) \mathrm{e}^{-\mathrm{i}z\sqrt{(\omega/c)^2-(\omega_0/c)^2\sin^2\xi}} \mathrm{e}^{\mathrm{i}\omega t} \mathrm{e}^{-T^2(\omega-\omega_0)^2}. \tag{15}$$

This polychromatic field retains its lateral Bessel profile but is time-limited along the direction of propagation. Because of the uniform time-windowing of the whole aperture plane, this pulsed Bessel beam does not acquire the X-shape characteristic of the X-waves [1] or the Bessel X-pulses [3]. Practically, such a pulse can be generated by a circular array using Bessel shading. The circular array manufactured by Lu and Greenleaf will produce a field similar

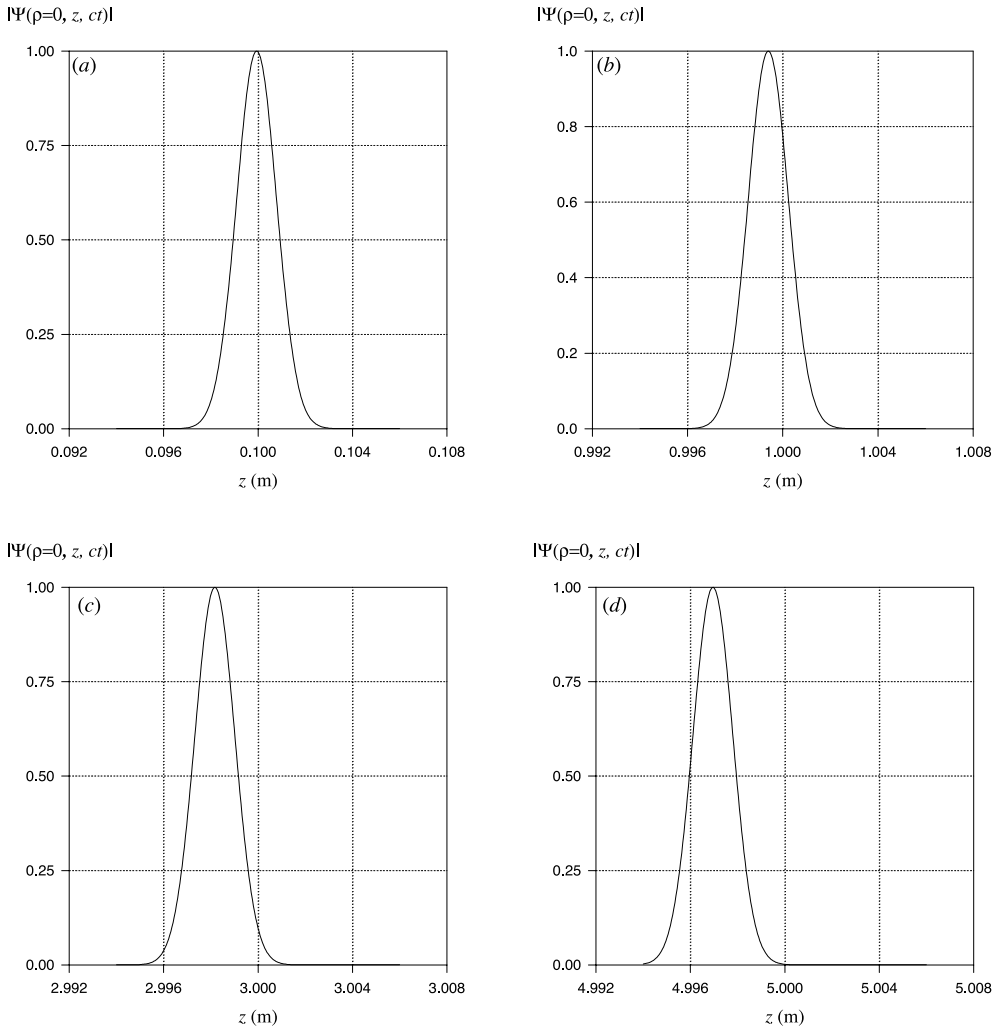

Figure 1. Axial time dependence of the envelope of a pulsed Bessel beam generated by applying a Gaussian temporal window uniformly over the source plane for $(\omega_0/c) = 4 \times 10^6$ m^{-1}, $cT = 0.0006$ m and $\xi = 2^\circ$. The pulses are observed at (*a*) $ct_0 = 0.1$ m, (*b*) $ct_0 = 1$ m, (*c*) $ct_0 = 3$ m and (*d*) $ct_0 = 5$ m.

to that given in equation (14) when all the array elements are pulsed using the same time-limiting function [8]. This excitation scheme is different from the successive excitation of the various array elements using different time sequences [2]. The uniformly pulsed Bessel beam has a peak travelling with a subluminal velocity $v < c$. This can be seen from figure 1, where the pulse given in equation (14) is plotted along the axis of propagation ($\rho = 0$) for $(\omega_0/c) = 4 \times 10^6$ m^{-1}, $cT = 0.0006$ m and $\xi = 2^\circ$. At observation times $ct_0 = 0.1$, 1, 3 and 5 m, the peak of the pulse occurs at $z_{\max} < ct_0$. The increase in the separation $ct_0 - z_{\max}$ indicates that the speed of the peak of the pulse is subluminal. This behaviour should be contrasted with the fact that the peak of the X-wave travels with a superluminal velocity $v > c$ [1, 6, 9]. The difference in the behaviour of these two pulsed Bessel beams is due to the nature of the temporal switching of the initial excitation.

2.2.2. Spatio-temporal X-shaped time window (I). In contrast to the uniform temporal switching of Bessel beams discussed in the preceding subsection, one can change the spatio-temporal distribution of the initial excitation. Consequently, different sections of the source could be pulsed at different times. From previous investigations, we know that smoothing the delta functions in the spectrum of a LW pulse corresponds to applying a time-window to the initial field excitation [6, 14–16, 51–54]. We use this property to describe an alternative method to produce pulsed Bessel beams. Starting with the Fourier spectrum of the monochromatic Bessel beam given in equations (3) and (4), we replace $\delta(\omega - \omega_0)$ by its limiting Gaussian function $\hat{\delta}(\omega - \omega_0)$, namely,

$$\hat{\delta}(\omega - \omega_0) = \left(T/\sqrt{\pi}\right)\mathrm{e}^{-T^2(\omega-\omega_0)^2}. \tag{16}$$

The corresponding Fourier spectrum is

$$\Phi_{\mathrm{F}}^{(2)}(\chi, \omega) = \left(2T\sqrt{\pi}/\chi\right)\mathrm{e}^{-T^2(\omega-\omega_0)^2}\delta(\chi - (\omega/c)\sin\xi). \tag{17}$$

Note that this spectrum has $\chi \propto (\omega/c)$ instead of having $\chi \propto (\omega_0/c)$ as in the spectrum derived in equation (13). The spectrum given in equation (17) exhibits the χ–ω coupling characteristic of LWs, while the one given in equation (13) does not. This χ–ω coupling reflects the intricate spatio-temporal character of the excitation wave fields of LWs. In the limit $T \to \infty$, both spectra given in equations (13) and (17) lead to the monochromatic Bessel beam given in equation (1).

At this point, we determine explicitly the shape of the excitation time window corresponding to the spectrum given in equation (17). This is done by evaluating the Hankel–Fourier transform, namely,

$$\Psi_p(\rho, z = 0, t) = (1/2\pi)\int_{-\infty}^{+\infty}\mathrm{d}\omega\int_0^{\infty}\mathrm{d}\chi\ \chi J_0(\chi\rho)$$
$$\times\mathrm{e}^{\mathrm{i}\omega t}\left(2T\sqrt{\pi}/\chi\right)\mathrm{e}^{-T^2(\omega-\omega_0)^2}\delta(\chi - (\omega/c)\sin\xi). \tag{18}$$

The integration over χ yields

$$\Psi_p(\rho, z = 0, t) = \left(T/\sqrt{\pi}\right)\int_{-\infty}^{+\infty}\mathrm{d}\omega\, J_0((\omega/c)\rho\sin\xi)\,\mathrm{e}^{\mathrm{i}\omega t}\mathrm{e}^{-T^2(\omega-\omega_0)^2}. \tag{19}$$

This integration over ω cannot be carried out to obtain a closed-form expression. However, one can have an idea of the shape of the time envelope of the initial excitation by evaluating the integration at specific ρ values. For example, at $\rho = 0$ the integration over ω yields the following initial illumination:

$$\Psi_p(\rho = 0, z = 0, t) = \mathrm{e}^{-(t^2/4T^2)}\mathrm{e}^{\mathrm{i}\omega_0 t}. \tag{20}$$

This is the same as the initial wave field given in equation (11) at $\rho = 0$. For $\rho \neq 0$, the resulting time-windows would be different. This can be seen for $\rho \neq 0$ by rewriting equation (19) as

$$\Psi_p(\rho, z = 0, t) = (cT/2\pi^3/2)\int_0^{2\pi}\mathrm{d}\phi\int_{-\infty}^{+\infty}\mathrm{d}k\,\mathrm{e}^{-\mathrm{i}k\rho\sin\xi\cos(\phi-\alpha)}\mathrm{e}^{\mathrm{i}kct}\mathrm{e}^{-c^2T^2(k-k_0)^2} \tag{21}$$

where $k = (\omega/c)$. The integration over k gives

$$\Psi_p(\rho, z = 0, t) = (1/2\pi)\int_0^{2\pi}\mathrm{d}\phi\,\mathrm{e}^{-(\rho\sin\xi\cos(\phi-\alpha)-ct)^2/4(cT^2)}\mathrm{e}^{-\mathrm{i}k_0(\rho\sin\xi\cos(\phi-\alpha)-ct)}. \tag{22}$$

The integration given in equation (22) is evaluated numerically using the following parameter values: $(\omega_0/c) = 4 \times 10^6\ \mathrm{m}^{-1}$, $cT = 0.0006$ m and $\xi = 2^\circ$. For $cT \gg 1/(\omega_0/c)$, the initial

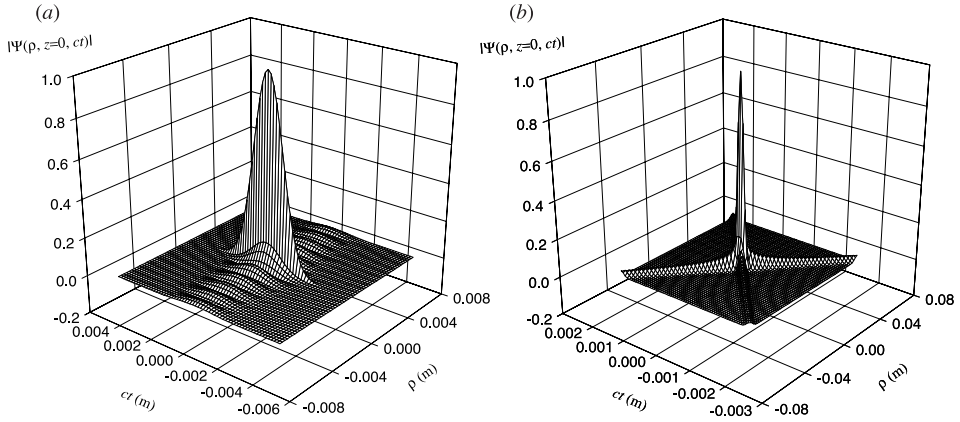

Figure 2. Surface plots of the initial excitation of a pulsed Bessel beams having an axicon angle $\xi = 2^\circ$ and characterized by the following parameter values: (*a*) $(\omega_0/c) = 4 \times 10^6$ m^{-1} and $cT = 0.0006$ m and; for which $cT \gg 1/(\omega_0/c)$. (*b*) $(\omega_0/c) = 1 \times 10^5$ m^{-1} and $cT = 6 \times 10^{-5}$ m; for which $cT \approx 1/(\omega_0/c)$.

excitation resembles that of a Bessel beam time-limited using a uniform Gaussian window. This is illustrated in figure 2(*a*), where a surface plot of the initial excitation is displayed for the chosen parameter values. On the other hand, the surface plot displayed in figure 2(*b*) for $(\omega_0/c) = 1 \times 10^5$ m^{-1}, $cT = 6 \times 10^{-5}$ m and $\xi = 2^\circ$ shows that for $cT \approx 1/(\omega_0/c)$ the excitation of the aperture acquires the X-armed shape characterizing the X-wave and the Bessel X-pulse [1, 3]. One should note that the central pulse of an X-wave field having $cT \gg 1/(\omega_0/c)$ contains a large number of oscillations, while for $cT \approx 1/(\omega_0/c)$ the number of oscillation is small. For $cT \gg 1/(\omega_0/c)$, the excitation given in equation (22) retains many properties of the X-shaped LWs although it looks like pulses produced by the uniform windowing scheme (cf equation (11)). Most notably, the peaks of the generated pulses propagate at superluminal instead of subluminal speeds.

2.2.3. Spatio-temporal X-shaped time window (II). Another finite-time window yielding a spectrum that reduces to equation (11) as $T \to \infty$ is the one used by Saari *et al* [3]. Their time-limiting function results from the use of a Fourier spectrum of the following form:

$$\Phi_{\mathrm{F}}^{(3)}(\chi, \omega) = \left(2T\sqrt{\pi/\chi}\right)\left(\sqrt{\omega}/\omega_0\right)\mathrm{e}^{-T^2(\omega-\omega_0)^2}\delta(\chi - (\omega/c)\sin\xi). \tag{23}$$

This spectrum has the advantage that it does not contain a non-oscillatory component $\left(\Phi_{\mathrm{F}}^{(3)}(\chi, \omega) = 0 \text{ at } \omega = 0\right)$. For such a spectrum, the radiated field can be evaluated using the following superposition:

$$\Psi_p(\rho, z, t) = (1/2\pi)\int_{-\infty}^{+\infty} \mathrm{d}\omega \int_0^{\infty} \mathrm{d}\chi\ \chi J_0(\chi\rho)\mathrm{e}^{-\mathrm{i}z\sqrt{(\omega/c)-\chi^2}}\mathrm{e}^{\mathrm{i}\omega t}\left(2T\sqrt{\pi}/\chi\right)$$
$$\times(\sqrt{\omega/\omega_0})\mathrm{e}^{-T^2(\omega-\omega_0)^2}\delta(\chi - (\omega/c)\sin\xi).$$

Carrying out the integration over χ and using $k = (\omega/c)$, we obtain

$$\Psi_p(\rho, z, t) = (cT/\sqrt{\pi})\int_{-\infty}^{+\infty} \mathrm{d}k\ (\sqrt{k/k_0})J_0(k\rho\sin\xi)\mathrm{e}^{+k(2c^2T^2k_0-\mathrm{i}u)}\mathrm{e}^{-c^2T^2k^2}\mathrm{e}^{-c^2T^2k_0^2} \tag{24}$$

where $u = z\cos\xi - ct$ and $k_0 = (\omega_0/c)$. Making use of the large argument approximation $I_0(x) \cong \mathrm{e}^x/\sqrt{2\pi x}$ and following the same procedure described by Saari [3], we arrive at the following approximate result:

$$\Psi_p(\rho, z, t) \cong \left(\sqrt{1 - \mathrm{i}(u/2k_0c^2T^2)}\right)\mathrm{e}^{-\mathrm{i}k_0u}\mathrm{e}^{-(u^2+\rho^2\sin^2\xi)/4c^2T^2}J_0((k_0 - \mathrm{i}(u/2c^2T^2))\rho\sin\xi).$$

This wavefield exhibits X-shaped arms similar to those of the X-wave. This can be seen for $(u/(2k_0c^2T^2)) \gg 1$; under this restriction, the above expression for $\Psi_p(\rho, z, t)$ can be approximated as follows:

$$\Psi_p(\rho, z, t) \cong \left(\sqrt{-\mathrm{i}u/2k_0c^2T^2}\right)\mathrm{e}^{-\mathrm{i}k_0u}\mathrm{e}^{-(u^2+\rho^2\sin^2\xi)/4c^2T^2}I_0(u\rho\sin\xi/2c^2T^2).$$

The approximation $I_0(x) \cong \mathrm{e}^x/\sqrt{2\pi x}$ gives, finally,

$$\Psi_p(\rho, z, t) \cong \left(\sqrt{-\mathrm{i}/2\pi k_0\rho\sin\xi}\right)\mathrm{e}^{-\mathrm{i}k_0u}\mathrm{e}^{-(u-\rho\sin\xi)^2/4c^2T^2}. \tag{25}$$

For distances $u \gg 2k_0c^2T^2$, the radiated field is exponentially small except for $u = \rho\sin\xi$. This relation between the values of u and ρ defines the X-shaped arms of the field of the Bessel X-pulse. The approximate expression given in equation (25) represents a pulse having a peak moving at a superluminal speed $c/\cos\xi$. The same superluminal propagation is achieved by other pulses deduced using different time windowing functions; for example, X-waves follow from using the initial time window $1/(a - \mathrm{i}ct)$ instead of the Gaussian window.

2.3. Pulsed Bessel beams generated by a circular array

In the preceding subsection, we considered three finite-time excitations of Bessel beams applied to infinite apertures. For a finite-size source having diameter D, the deduced results are essentially valid over a finite distance in the near-field range characterized by the limit $z_d = D/(2\tan\xi)$. The decay of pulsed Bessel beams and X-shaped LWs due to the finiteness of the size of the source has been considered in previous publications [14–16, 51–54, 60, 61]. However, we provide an expression for the field radiated by an array of N annular rings when the field given in equation (24) is used as an initial excitation. Specifically,

$$\Psi_p(\rho = 0, z, t) = \sum_{n=1}^{N} \frac{\mathrm{i}cT\rho_n'\Delta\rho'}{\sqrt{\pi(\rho_n'^2 + z^2)}} \int_{-\infty}^{+\infty} \mathrm{d}k\, k\cos\xi(\sqrt{k/k_0})J_0(k\rho_n'\sin\xi)$$
$$\times \mathrm{e}^{-c^2T^2(k-k_0)^2}\mathrm{e}^{-\mathrm{i}k\sqrt{\rho_n'^2+z^2}}\mathrm{e}^{\mathrm{i}kct} \tag{26}$$

where $\Delta\rho'$ is the separation between the array elements, $\rho_n' = n\Delta\rho'$ gives the radial position of each ring and the finite radius of source is given by $(D/2) = N\Delta\rho'$. This expression follows from applying the Rayleigh–Sommerfeld formula (6) to a discretized circular aperture. The on-axis amplitude of the pulse radiated from a discretized aperture consisting of $N = 500$ elements is shown in figure 3 at observation times $ct_0 = 0.3$, 0.8, 1.3 and 1.8 m. The radiating source has a radius $(D/2) = 0.05$ m, central angular frequency $(\omega_0/c) = 2 \times 10^4\ \mathrm{m}^{-1}$, pulse duration $cT = 0.006$ m and axicon angle $\xi = 4^\circ$. One should note that the centre of the pulse occurs at distances $z_{\max} > ct_0$. The increase in the separation $(z_{\max} - ct_0)$ as the pulse travels away from the source indicates that the speed of the peak of the pulse is superluminal. The onset of the fast decay of the peak amplitude occurs at $z_d = D/(2\tan\xi) = 0.715$ m, as can be seen from the large drop in the field amplitude between $ct_0 = 0.8$ and 1.3 m illustrated in figures 3(*b*) and (*c*).

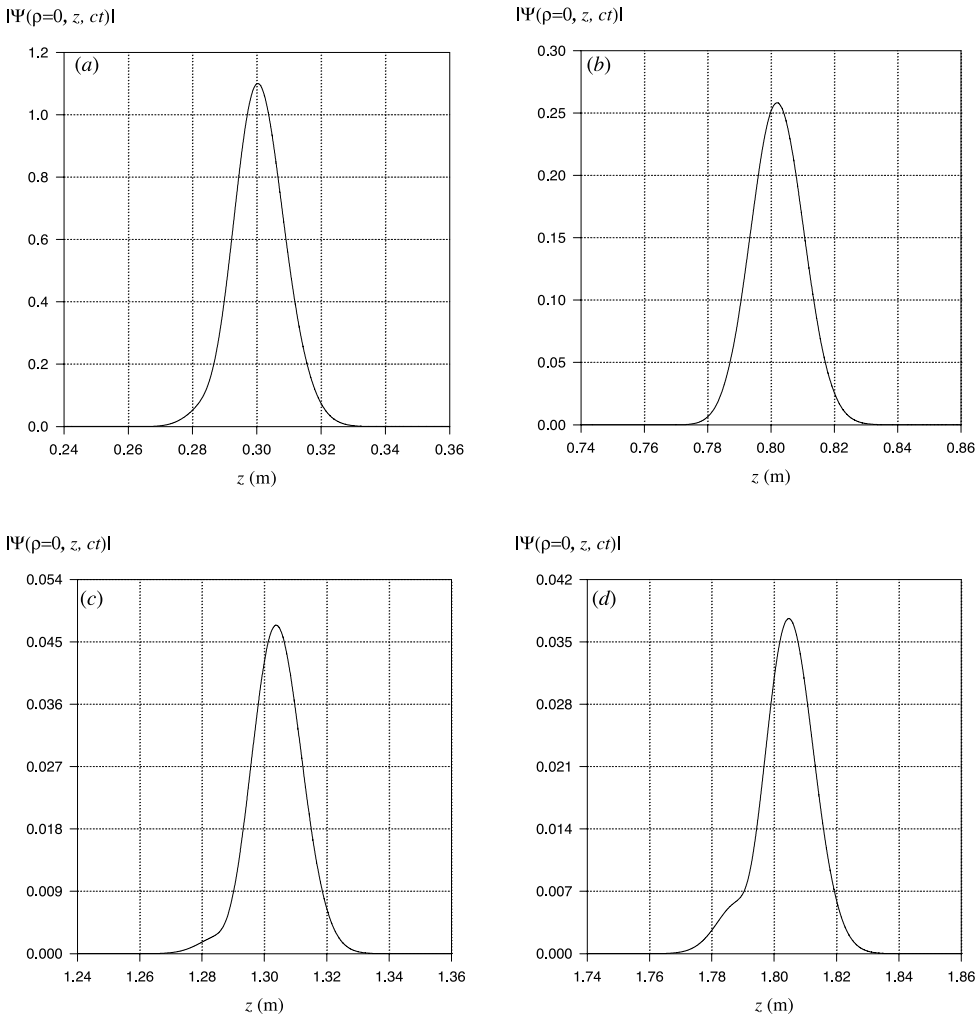

Figure 3. Axial envelope of a pulsed Bessel beam radiated from a discrete aperture consisting of $N = 500$ elements and having $(D/2) = 0.05$ m, $(\omega_0/c) = 2 \times 10^4$ m^{-1}, $cT = 0.006$ m and $\xi = 4^\circ$. The pulse is plotted at observation times: (*a*) $ct_0 = 0.3$ m; (*b*) $ct_0 = 0.8$ m; (*c*) $ct_0 = 1.3$ m; and (*d*) $ct_0 = 1.8$ m.

3. Pulsed Bessel beams generated by an annular slit

In the preceding section, we have shown that X-shaped waves can be generated from a flat aperture given that various sections of the aperture are excited using different time sequences. In practical situations, this can be achieved using circular arrays having independently addressable discrete elements [2]. It has been established, however, that Bessel beams can be generated using other methods [23–33]. In this section, we consider the generation of pulsed Bessel beams by applying a uniform pulsed illumination to a thin annular slit. This method is viable because the Fraunhofer diffraction image of an annular slit has a Bessel transverse radial dependence. An annular slit having a finite width, thus, produces a finite-energy approximation of the Bessel beam.

3.1. Monochromatic Bessel beams generated by an annular slit

The field generated from a thin annular slit can be calculated using the Rayleigh–Sommerfeld expression given in equation (6) with $(D_1/2) < \rho' < (D_2/2)$. Along such vein, consider the uniform illumination

$$\Psi(\rho', z', t') = \Psi_0 \mathrm{e}^{-\mathrm{i}k_0(z'-ct')}$$

where $k_0 = (\omega_0/c)$. If the annular slit is opened in a screen situated at $z = 0$, the derivative with respect to the normal to the aperture plane is given by

$$(\partial\Psi(\rho', z', t')/\partial z')\big|_{z'=0} = -\mathrm{i}k_0\Psi_0 \mathrm{e}^{\mathrm{i}\omega_0 t}\mathrm{e}^{-\mathrm{i}(\omega_0/c)R}.$$

The Rayleigh–Sommerfeld formula gives the generated field for $z > 0$. Using equation (8), we obtain

$$\Psi(\rho, z, t) = (\mathrm{i}\omega_0\Psi_0/2\pi c)\int_0^{2\pi}\mathrm{d}\phi'\int_{(D_1/2)}^{(D_2/2)}\mathrm{d}\rho'\,\rho'\mathrm{e}^{\mathrm{i}\omega_0 t}(1/\pi)$$
$$\times\int_0^{\infty}\mathrm{d}\lambda\,\lambda\int_{-\infty}^{+\infty}\mathrm{d}k_z\,J_0(\lambda\rho^*)\frac{\mathrm{e}^{-\mathrm{i}k_z z}}{k_z^2 - ((\omega_0/c)^2 - \lambda^2)}.$$

The integration over ϕ' and k_z yields

$$\Psi(\rho, z, t) = (\mathrm{i}\omega_0\Psi_0/2\pi c)\int_{(D_1/2)}^{(D_2/2)}\mathrm{d}\rho'\,\rho'\mathrm{e}^{\mathrm{i}\omega_0 t}$$
$$\times\int_0^{\infty}\mathrm{d}\lambda\,\lambda(-2\pi\mathrm{i})J_0(\lambda\rho)J_0(\lambda\rho')\frac{\mathrm{e}^{-\mathrm{i}z\sqrt{(\omega_0/c)^2-\lambda^2}}}{\sqrt{(\omega_0/c)^2-\lambda^2}}. \tag{27}$$

The integration over ρ'in equation (27) is carried out, yielding

$$\Psi(\rho, z, t) = (\omega_0\Psi_0/c)\int_0^{\infty}\mathrm{d}\lambda\left\{(D_2/2)J_1(\lambda D_2/2) - (D_1/2)J_1(\lambda D_1/2)\right\}$$
$$\times J_0(\lambda\rho)\frac{\mathrm{e}^{-\mathrm{i}z\sqrt{(\omega_0/c)^2-\lambda^2}}}{\sqrt{(\omega_0/c)^2-\lambda^2}}\mathrm{e}^{\mathrm{i}\omega_0 t}. \tag{28}$$

Introducing the new variable $\phi = \phi_R + \mathrm{i}\phi_I$ defined by the transformation $\lambda = k_0\sin\phi$, we obtain [55]

$$\Psi(\rho, z, t) = (\omega_0\Psi_0/c)\int_0^{(\pi/2)}\mathrm{d}\phi_R\big\{(D_2/2)J_1(k_0\sin\phi_R(D_2/2))$$
$$-(D_1/2)J_1(k_0\sin\phi_R(D_1/2))\big\}J_0(k_0\rho\sin\phi_R)\mathrm{e}^{-\mathrm{i}k_0(z\cos\phi_R - ct)}$$
$$+(\omega_0\Psi_0/c)\int_0^{\infty}\mathrm{d}\phi_I\big\{(D_2/2)J_1(k_0\cosh\phi_I(D_2/2))$$
$$-(D_1/2)J_0(k_0\rho\cosh\phi_I(D_1/2))\big\}J_0(k_0\rho\cosh\phi_I)\mathrm{e}^{-\mathrm{i}k_0 z\sinh\phi_I}\mathrm{e}^{\mathrm{i}\omega_0 t}. \tag{29}$$

The first integration on the right-hand side corresponds to the radiated field. We can have an idea of how the result of the integration behaves using the stationary phase method. This is particularly true for optical applications where the frequency of the illumination field $(\omega_0/c) \approx 10^7$ m is very large. The two terms $J_1((\omega_0/c)\sin\phi_R(D_1/2))$ and $J_1((\omega_0/c)\sin\phi_R(D_2/2))$ can be approximated by making use of the corresponding large-argument asymptotic expressions [59]. The integrand, thus, contains highly oscillatory terms with an exponential dependence

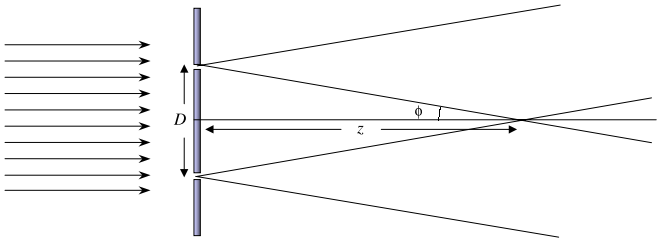

Figure 4. Stationary angle $\phi_R^{(s)} = \arctan(D/2z)$ suspended by the annular ring on an observation point lying on the axis of propagation.

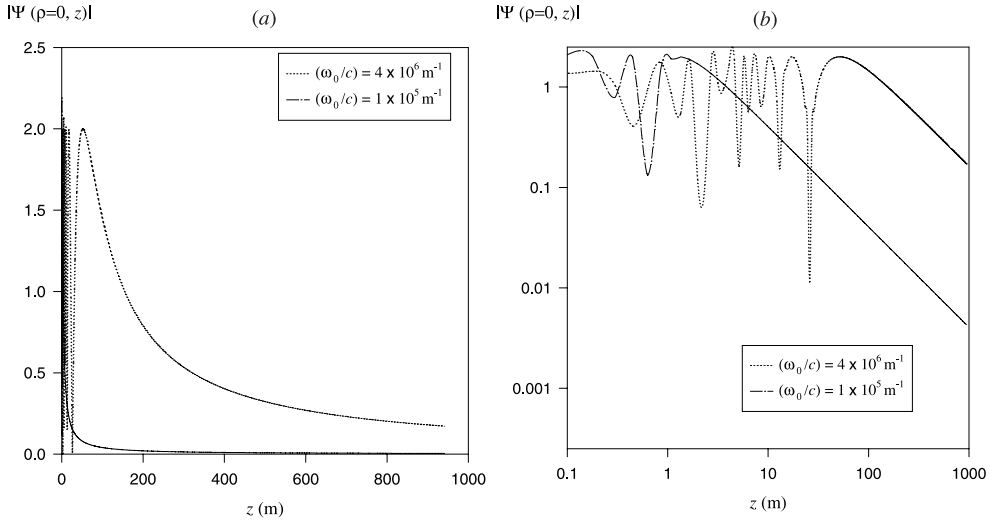

Figure 5. Decay of monochromatic Bessel beams generated using an annular slit for the two frequencies $(\omega_0/c) = 4 \times 10^6$ m^{-1} and $(\omega_0/c) = 1 \times 10^5$ m^{-1}. The inner and outer radii of the slit are chosen to equal $(D_1/2) = 0.04$ m and $(D_2/2) = 0.041$ m. The decay in the amplitude versus the distance from the source is plotted using (*a*) normal and (*b*) log–log scales.

$\exp(\pm \mathrm{i}(\omega_0/c) \sin \phi_R (D_j/2))$, where $j = 1$ or 2. The stationary phase method indicates that the main contribution to such highly oscillatory integration occurs when

$$(\partial/\partial\phi_R)((\omega_0/c)z \cos\phi_R \pm (\omega_0/c)(D_j/2) \sin\phi_R) = 0$$

for which

$$\tan\phi_R^{(s)} = \pm(D_j/2z)$$

where $j = 1$ or 2. For a narrow slit $D_1 \approx D_2 = D$, the stationary angle $\phi_R^{(s)} = \arctan(D/2z)$ corresponds to the angle suspended by the annular ring on an observation point lying on the axis of propagation as shown in figure 4. Thus, unlike the planar excitation discussed in section 2, the angle $\phi_R^{(s)}$ (equivalent to the axicon angle ξ) depends on the observation point and is not a constant parameter.

Along the axis of propagation, an exact expression for the generated field can be derived by direct integration of equation (27)

$$\Psi(\rho = 0, z, t) = \mathrm{i}(\omega_0 \Psi_0/2\pi c) \int_0^{2\pi} \mathrm{d}\phi' \int_{(D_1/2)}^{(D_2/2)} \mathrm{d}\rho' \rho' \mathrm{e}^{\mathrm{i}\omega_0 t} \frac{\mathrm{e}^{-\mathrm{i}(\omega_0/c)\sqrt{\rho'^2+z^2}}}{\sqrt{\rho'^2+z^2}}.$$

The integration over ϕ' and ρ' gives

$$\Psi(\rho = 0, z, t) = -\Psi_0\left(\mathrm{e}^{-\mathrm{i}(\omega_0/c)(\sqrt{(D_2/2)^2+z^2}-ct)} - \mathrm{e}^{-\mathrm{i}(\omega_0/c)(\sqrt{(D_1/2)^2+z}-ct)}\right) \tag{30}$$

which is the difference between two outgoing plane waves emerging from the edges at $(D_1/2)$ and $(D_2/2)$ [62]. The decay behaviour of such a field is shown in figure 5 for $(\omega_0/c) = 4 \times 10^6$ m^{-1} and $(\omega_0/c) = 1 \times 10^5$ m^{-1}. For both frequencies, the inner and outer radii of the slit are chosen to equal $(D_1/2) = 0.04$ m and $(D_2/2) = 0.041$ m, respectively. Figure 5(*a*) illustrates the fast decay of the field corresponding to $(\omega_0/c) = 1 \times 10^5$ m^{-1} due of its shorter Rayleigh diffraction limit. In figure 5(*b*), a log–log plot of the amplitude $|\Psi(\rho = 0, z, t)|$ versus the distance z shows that the fields entering the far-field range exhibit the typical $(1/z)$ decay.

3.2. Pulsed Bessel beams generated by an annular slit

Consider the case of a pulsed illumination of the annular slit. We assume that the time-limited initial illumination is given as follows:

$$\Psi_i(\rho, z = 0, t) = \Psi_0 \int_0^\infty \mathrm{d}\omega\, (\omega/\omega_0)\left(T/\sqrt{\pi}\right)\mathrm{e}^{-(\omega-\omega_0)^2T^2}\mathrm{e}^{\mathrm{i}\omega t}\mathrm{e}^{-\mathrm{i}(\omega/c)z}\big|_{z=0}. \tag{31}$$

Hence, we are dealing with the same problem discussed in the preceding section. The only difference is that the result obtained for a monochromatic illumination has to be integrated over the Gaussian spectrum chosen in equation (31). Note that the spectrum includes an (ω/ω_0) term to ensure that non-oscillatory terms do not contribute to the spectrum of the generated wave. Using equation (28), the pulse generated by the annular slit is written as

$$\Psi_p(\rho, z, t) = (\Psi_0/c)\int_0^\infty \mathrm{d}\omega \int_0^\infty \mathrm{d}\chi\left(\omega^2T/\omega_0\sqrt{\pi}\right)\mathrm{e}^{-(\omega-\omega_0)^2T^2}J_0(\chi\rho)$$
$$\times\left\{(D_2/2)J_1(\chi(D_2/2)) - (D_1/2)J_1(\chi D_1/2)\right\}\frac{\mathrm{e}^{-\mathrm{i}z\sqrt{(\omega/c)^2-\chi^2}}}{\sqrt{(\omega/c)^2-\chi^2}}\mathrm{e}^{\mathrm{i}\omega t}. \tag{32}$$

Along the axis of propagation, the amplitude of the monochromatic Bessel beam given in equation (30) is used to derive a closed-form expression for the amplitude of the radiated pulse, namely,

$$\Psi_p(\rho = 0, z, t) = -\Psi_0\int_0^\infty \mathrm{d}\omega\,(\omega/\omega_0)\left(T/\sqrt{\pi}\right)\mathrm{e}^{-(\omega-\omega_0)^2T^2}\left\{\mathrm{e}^{-\mathrm{i}(\omega/c)(\sqrt{(D_2/2)^2+z^2}-ct)}\right.$$
$$\left.-\mathrm{e}^{-\mathrm{i}(\omega/c)(\sqrt{(D_1/2)^2+z^2}-ct)}\right\}. \tag{33}$$

This expression is the difference between two integrations representing the contributions from the two edges of the slit. For large ω_0 values, we can extend the limits of the above integration to $-\infty \to +\infty$. The identity (3.462.6) in [63] is then used to evaluate the integration over ω giving the following field amplitude along the axis of propagation:

$$\Psi_p(\rho = 0, z, t) = -\Psi_0(1/(\omega_0T)^2)\left\{(\omega_0T)^2 - \mathrm{i}(\omega_0/2c)\left(\sqrt{(D_2/2)^2+z^2} - ct\right)\right\}$$
$$\times\mathrm{e}^{-(\sqrt{(D_2/2)^2+z^2}-ct)^2/4c^2T^2}\mathrm{e}^{-\mathrm{i}(\omega_0/c)(\sqrt{(D_2/2)^2+z^2}-ct)}$$
$$+\Psi_0(1/(\omega_0T)^2)\left\{(\omega_0T)^2 - \mathrm{i}(\omega_0/2c)\left(\sqrt{(D_1/2)^2+z^2} - ct\right)\right\}$$
$$\times\mathrm{e}^{-(\sqrt{(D_1/2)^2+z^2}-ct)^2/4c^2T^2}\mathrm{e}^{-\mathrm{i}(\omega_0/c)(\sqrt{(D_1/2)^2+z^2}-ct)}. \tag{34}$$

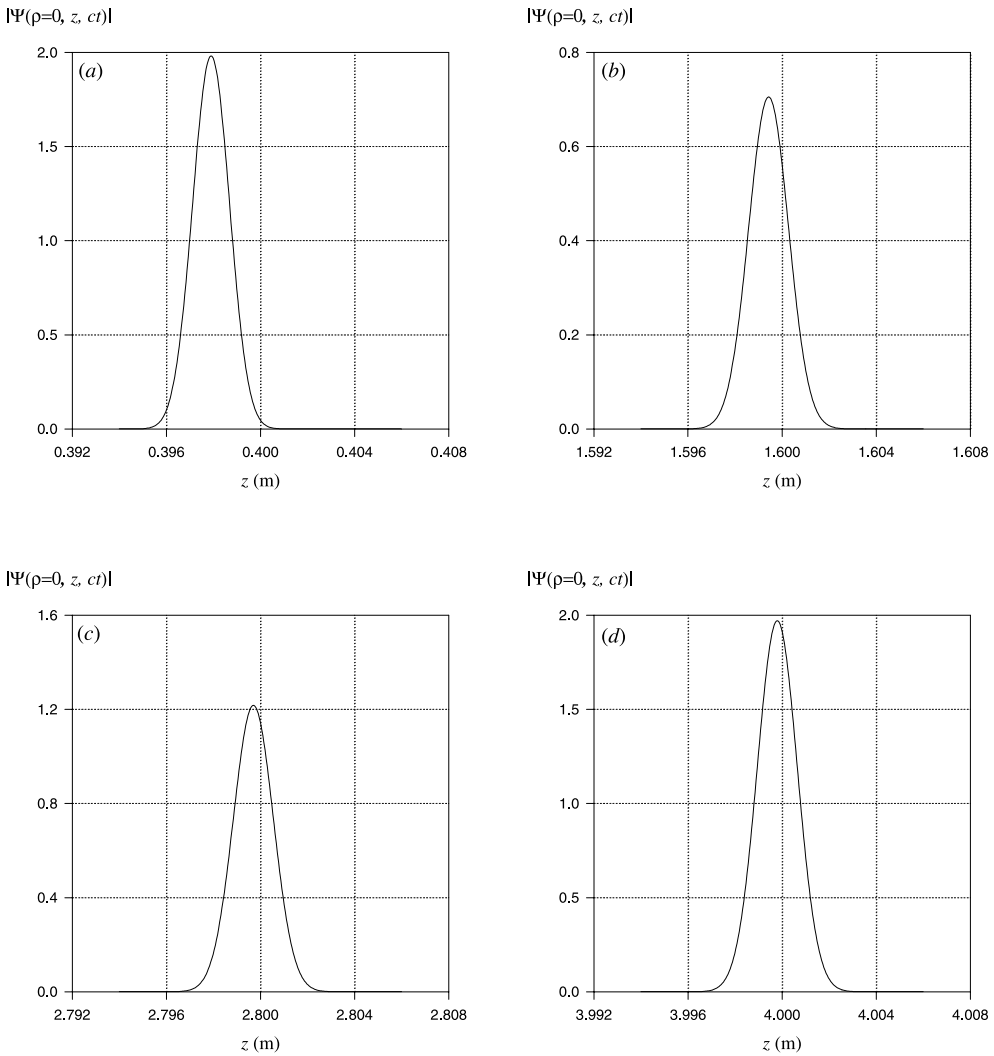

Figure 6. Axial time envelope of a pulsed Bessel beam generated by an annular slit plotted for $(\omega_0/c) = 4 \times 10^6$ m^{-1}, $cT = 0.0006$ m, $(D_1/2) = 0.04$ m and $(D_2/2) = 0.041$ m. The pulse is displayed at observation times: (*a*) $ct_0 = 0.4$; (*b*) $ct_0 = 1.6$ m; (*c*) $ct_0 = 2.8$ m; and (*d*) $ct_0 = 4$ m.

This pulse consists of two terms each having a pulsed envelope with a centre moving with speed

$$\frac{z(\mathrm{d}z/\mathrm{d}t)}{\sqrt{(D/2)^2 + z^2}} = c$$

or

$$v_g = \frac{\mathrm{d}z}{\mathrm{d}t} = c\frac{\sqrt{(D/2)^2 + z^2}}{z}.$$

The group velocity is evaluated using $\mathrm{d}\left(\sqrt{(D/2)^2 + z^2} - ct\right)/\mathrm{d}t = 0$. The speed of the centre of the generated pulse is superluminal. However, the velocity decreases as the pulse travels

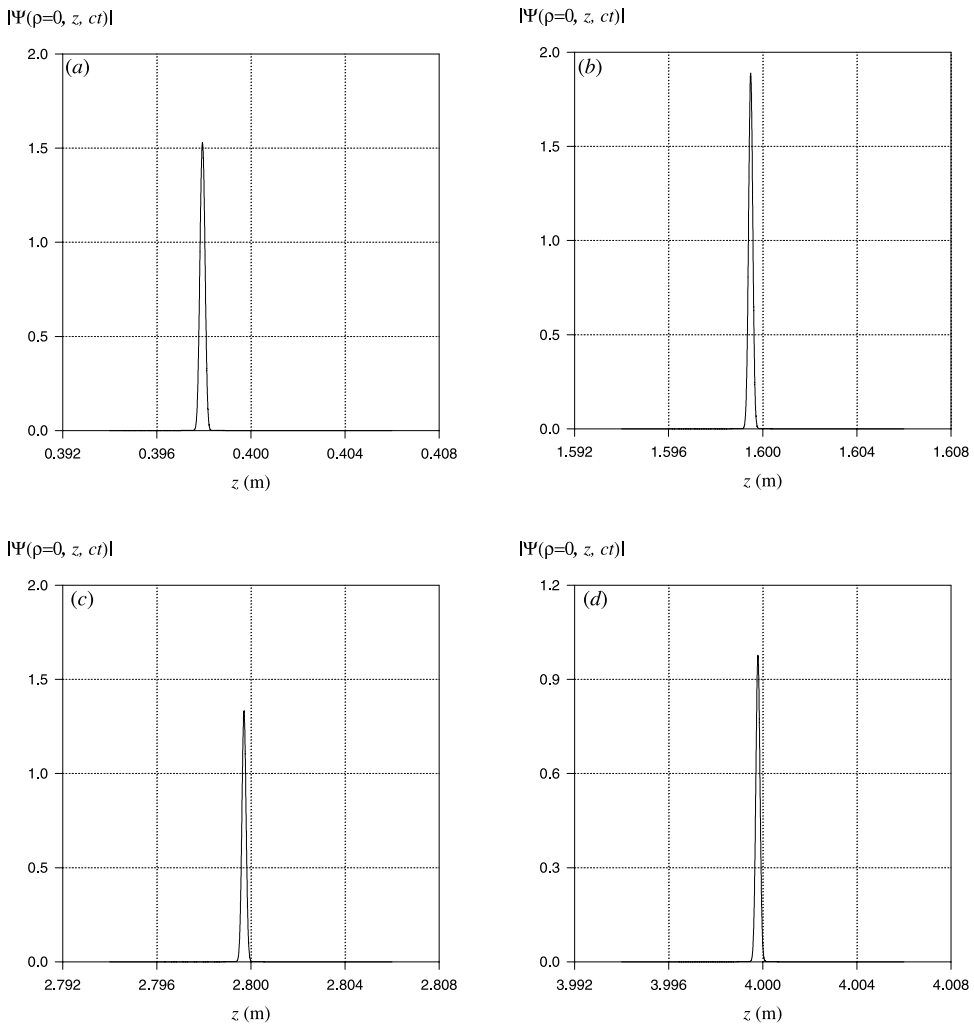

Figure 7. Same as in figure 6 but the axial time envelope of the pulsed Bessel beam is plotted for $(\omega_0/c) = 1 \times 10^5$ m^{-1} and $cT = 6 \times 10^{-5}$ m.

further. This effect is due to a 'delayed launching' effect. The pulse launched at $ct = (D/2)$ takes a time equal to $\left(\left(\sqrt{z_0^2 + (D/2)^2} - (D/2)\right)/c\right) < (z_0/c)$ to reach a distance z_0. Thus, the pulse appears to have travelled at a velocity $v > c$. The same conclusion is reached when we consider the time evolution of the envelope of the pulse plotted in figure 6 for $(\omega_0/c) = 4 \times 10^6$ m^{-1}, $cT = 0.0006$ m, $(D_1/2) = 0.04$ m and $(D_2/2) = 0.041$ m. It is clear that the peak of the pulse plotted at $ct_0 = 0.4$, 1.6, 2.8 and 4 m moves at a speed larger than c. To clarify this point, we have plotted in figure 8 the positions of the peak of the pulse at different observation times. The negative sign of $z_{\max} - ct_0$ indicates that the peak of a pulsed Bessel beam is lagging behind the position $z_0 = ct_0$ defining the peak of a pulse travelling at the speed of light. This means that, globally, the peak of the pulsed Bessel beam will not overtake that of a pulse travelling at the speed of light. However, locally, a pulsed Bessel Beam travels at a superluminal velocity in the near field of the

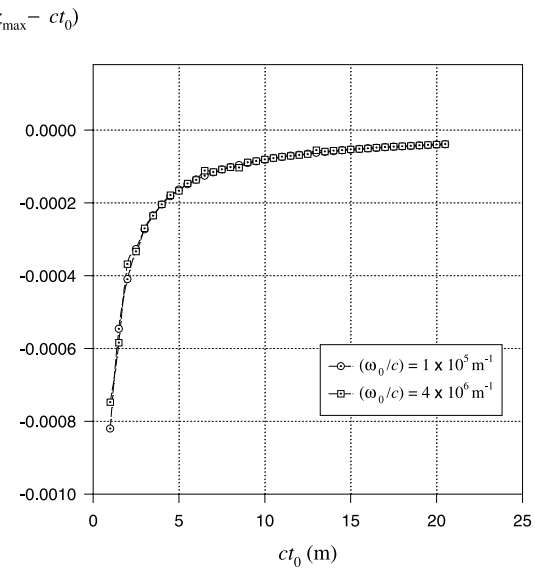

Figure 8. Positions of the peaks of the pulsed Bessel beams generated by an annular slit at different observation times. The positions of the peaks are plotted for the two frequencies $(\omega_0/c) = 4 \times 10^6$ m^{-1} and $(\omega_0/c) = 1 \times 10^5$ m^{-1}.

aperture. This can be deduced from the slope of the curve given in figure 8. The larger slopes indicate that the velocity of the peak of the field is much larger than c. As the curve levels up, the velocity of the pulse as it traverses a distance between any two successive points approaches c. In the far-field range, the velocity of the peak of the pulsed Bessel beam becomes equal to the speed of light. Henceforth, the position of the peak is located at $z_0 = ct_0$. One could argue that the superluminal advancement in the position of the peak of the pulse shown in figure 6 is slight in comparison to the axial width of the pulse itself. Therefore, the observability of such effect would be difficult. In figure 7, we plot the pulsed Bessel beams generated for $(\omega_0/c) = 1 \times 10^5$ m^{-1} and $cT = 0.000\,06$ m. This X-shaped pulse has a much shorter axial width. Therefore, the observability of the superluminal propagation of this pulse is enhanced in comparison to the case illustrated in figure 6. One should note, however, that the positions of the peak of the pulse at different times are comparable to the case of a pulse having a longer axial width. This can be seen by comparing the two curves in figure 8 showing the positions of the peaks of the two pulsed Bessel beams.

4. Pulsed Bessel beams generated by axicons

In this section, we investigate the possibility of using an axicon to create a superluminal X-shaped pulse. An axicon is a conical lens that contributes to the emerging field components a relative phase delay having a linear dependence on the radial coordinate ρ'. Such a conical lens will be referred to as a refractive axicon. In contrast, a diffractive axicon is a holographic element designed to introduce a linear phase delay using a circular grating. We study the two types of optical elements and demonstrate that the refractive axicon produces superluminal X-shaped pulses. The diffractive axicon produces pulses that initially propagate at subluminal velocities near the source. As the latter travel further away from the source, their speeds become superluminal.

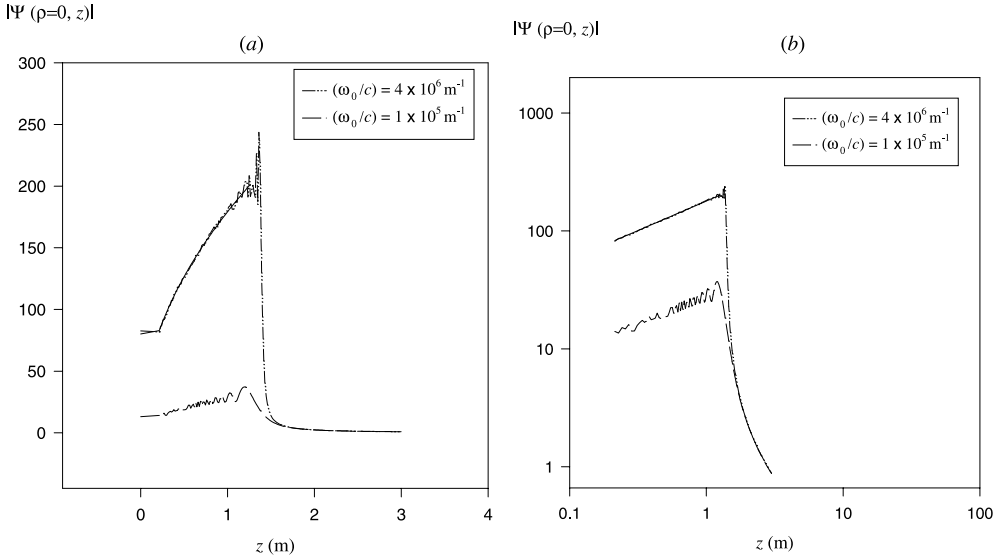

Figure 9. Decay of monochromatic Bessel beams generated using an axicon for the two frequencies $(\omega_0/c) = 4 \times 10^6$ m^{-1} and $(\omega_0/c) = 1 \times 10^5$ m^{-1}. The radius of the axicon is equals $(D/2) = 0.05$ m and $\gamma = 28$. The decay in the amplitude versus the distance is displayed using (*a*) normal and (*b*) log–log scales.

4.1. Monochromatic Bessel beam generated by axicons

Consider a continuous-wave monochromatic illumination of an axicon. For high frequencies, the influence of an axicon can be approximated by a phase factor having a linear dependence on ρ'. Specifically, the generated field resulting from a monochromatic plane wave illumination of an axicon is given as

$$\Psi(\rho, z, t) = -(\mathrm{i}\omega_0\Psi_0/2\pi c)\int_0^{(D/2)} \mathrm{d}\rho'\,\rho' \mathrm{e}^{\mathrm{i}\omega_0 t}\int_0^{\infty} \mathrm{d}\lambda\,\lambda(2\pi\mathrm{i})J_0(\lambda\rho)J_0(\lambda\rho')$$

$$\times \frac{\mathrm{e}^{-\mathrm{i}z\sqrt{(\omega_0/c)^2-\lambda^2}}}{\sqrt{(\omega_0/c)^2-\lambda^2}}\mathrm{e}^{+\mathrm{i}(\omega_0/c)(\rho'/\gamma)}. \tag{35}$$

The parameter γ is related to the axicon angle ξ and the refractive index n through the relationship $(1/\gamma) = (n-1)\tan\xi$ [26, 29]. The above integration is deduced using a procedure similar to that leading to equation (27). Along the axis of propagation the generated field reduces to

$$\Psi(\rho = 0, z, t) = -(\mathrm{i}\omega_0\Psi_0/2\pi c)\int_0^{(D/2)} \mathrm{d}\rho'\,\rho' \mathrm{e}^{\mathrm{i}\omega_0 t}\int_0^{\infty} \mathrm{d}\lambda\,\lambda(2\pi\mathrm{i})J_0(\lambda\rho')$$

$$\times \frac{\mathrm{e}^{-\mathrm{i}z\sqrt{(\omega_0/c)^2-\lambda^2}}}{\sqrt{(\omega_0/c)^2-\lambda^2}}\mathrm{e}^{+\mathrm{i}(\omega_0/c)(\rho'/\gamma)}. \tag{36}$$

The integration over λ yields

$$\Psi(\rho = 0, z, t) = \mathrm{i}(\omega_0/c)\Psi_0\int_0^{(D/2)} \mathrm{d}\rho'\,\rho' \mathrm{e}^{\mathrm{i}\omega_0 t}\frac{\mathrm{e}^{\mathrm{i}(\omega_0/c)\rho'/\gamma}}{\sqrt{z^2+\rho'^2}}\mathrm{e}^{-\mathrm{i}(\omega_0/c)\sqrt{z^2+\rho'^2}}. \tag{37}$$

This expression is integrated numerically and plotted in figures 9(*a*) and (*b*) for normal and logarithmic scales, respectively. The two figures illustrate the decay patterns corresponding to $(\omega_0/c) = 4 \times 10^6$ m^{-1} and $(\omega_0/c) = 1 \times 10^5$ m^{-1}. The radius of the axicon is chosen to equal $(D/2) = 0.05$ m and $\gamma = 28$. The fast decay of the two Bessel beams generated by an axicon starts at the same distance independently of the frequency. The reason for this frequency independence is that the near-far field limit of the Bessel beam equals $(D/2)\gamma$. In the derivation of this near-far field limit, the waist of the beam ($\propto 1/(\omega_0/c)$) offsets the effect of operating at a higher frequency [16, 53, 61]. Figure 9(*b*) shows that following the initial fast decay of the field amplitude, the rate of decay starts slowing down and approaches asymptotically the $1/z$ roll-off.

For high-frequency monochromatic illumination, the method of stationary phase can be used for evaluating the integration in equation (37). The phase of the integrand is equal to

$$\Theta(\rho') = (\rho'/\gamma) - \sqrt{z^2 + \rho'^2}.$$

The stationary phase condition $(\partial\Theta(\rho')/\partial\rho') = (1/\gamma) - \left(\rho'/\sqrt{z^2 + \rho'^2}\right) = 0$ is applied using equation (6.5.12) in [64] to obtain

$$\Psi(\rho = 0, z, t) \approx \mathrm{i}\sqrt{2\pi\gamma(\omega_0/c)}\Psi_0 \mathrm{e}^{-\mathrm{i}(\omega_0/c)\left(\left(\sqrt{\gamma^2-1}/\gamma\right)z - ct\right)}\left(\sqrt{z}/(\gamma^2-1)^{3/4}\right)\mathrm{e}^{-\mathrm{i}(\pi/4)} \tag{38}$$

for $0 < z < (D/2)\sqrt{\gamma^2 - 1}$.

The intensity of the generated beam increases with z in the near-field range. For the far-field range, when $z > (D/2)\sqrt{\gamma^2 - 1}$, the leading-order term is deduced using partial integration; specifically,

$$\Psi(\rho = 0, z, t) \approx \Psi_0 \frac{(D/2)}{\left((1/\gamma)\sqrt{(D/2)^2 + z^2} - (D/2)\right)} \mathrm{e}^{-\mathrm{i}(\omega_0/c)\left(\sqrt{z^2+(D/2)^2} - ct\right)} \mathrm{e}^{\mathrm{i}(\omega_0/c)(D/2\gamma)} \tag{39}$$

for $z > (D/2)\sqrt{\gamma^2 - 1}$. One should note that the analysis presented here is valid for both refractive and diffractive axicons. This is the case because we are dealing with a single frequency and the circular grating is designed for that particular frequency. The asymptotic near-field expression given in equation (38) for $(\omega_0/c) = 4 \times 10^6$ m^{-1} is shown as a full curve in figures 9(*a*) and (*b*). These figures display the characteristic $\sqrt{z}$ increase in the amplitude of the pulsed Bessel beam in the near field.

4.2. Pulsed Bessel beam generated by a refractive axicon

For a uniform pulsed illumination of the axicon, we use the same procedure described in the preceding sections. The initial pulsed illumination is the same as that given in equation (31). The on-axis amplitude of a pulsed Bessel beam generated using an axicon is, thus, a Fourier superposition with spectral amplitudes are given by the expression (37); specifically,

$$\Psi_p(\rho = 0, z, t) = \frac{\mathrm{i}\Psi_0}{(\omega_0/c)} \int_0^{(D/2)} \mathrm{d}\rho' \, \frac{\rho'}{\sqrt{z^2 + \rho'^2}} \int_0^{\infty} \mathrm{d}(\omega/c)\,(\omega/c)^2 \left(cT/\sqrt{\pi}\right)\mathrm{e}^{-(\omega-\omega_0)^2T^2}$$
$$\times \mathrm{e}^{+\mathrm{i}\omega t}\mathrm{e}^{-\mathrm{i}(\omega/c)\sqrt{z^2+\rho'^2}}\mathrm{e}^{\mathrm{i}(\omega/c)(\rho'/\gamma)}. \tag{40}$$

For large ω_0, the integration over (ω/c) can be approximated by an integration having limits that extend from $-\infty \to +\infty$ because contributions from negative ω values are exponentially

small. Using formula (3.462.8) in [63], we integrate over (ω/c) to obtain the following amplitude for the on-axis field:

$$\Psi_p(\rho=0,z,t) \cong \mathrm{i}\Psi_0 \int_0^{(D/2)} \mathrm{d}\rho' \, \frac{\rho'}{\sqrt{z^2+\rho'^2}} \mathrm{e}^{-(\sqrt{z^2+\rho'^2}-(\rho'/\gamma)-ct)^2/4c^2T^2} \times \mathrm{e}^{-\mathrm{i}(\omega_0/c)(\sqrt{z^2+\rho'^2}-(\rho'/\gamma)-ct)}(\omega_0/c) \times \left\{1+2\left(\omega_0 T-(\mathrm{i}/2cT)\left(\sqrt{z^2+\rho'^2}-\left(\rho'/\gamma\right)-ct\right)\right)^2\right\}/2(\omega_0 T)^2. \tag{41}$$

The leading order of this integration can be evaluated using the stationary phase analysis applied previously to the case of monochromatic illumination. The stationary phase method leads to the following expression for the axicon-generated pulsed Bessel beam:

$$\Psi_p(\rho=0,z,t) \approx \mathrm{i}\Psi_0\sqrt{2\pi\gamma(\omega_0/c)}\,\mathrm{e}^{-(z(\sqrt{\gamma^2-1}/\gamma)-ct)^2/4c^2T^2}\mathrm{e}^{-\mathrm{i}(\omega_0/c)(z(\sqrt{\gamma^2-1}/\gamma)-ct)}\mathrm{e}^{-\mathrm{i}(\pi/4)} \times \left(\sqrt{z}/(\gamma^2-1)^{3/4}\right)\left\{1+2\left(\omega_0 T-(\mathrm{i}/2cT)\left(z\left(\sqrt{\gamma^2-1}/\gamma\right)-ct\right)\right)^2\right\}/2(\omega_0 T)^2 \tag{42}$$

for $0 < z < (D/2)\sqrt{\gamma^2-1}$. This pulse has a Gaussian axial width and a centre moving at a superluminal velocity $v_p = (\gamma/\sqrt{\gamma^2-1})c$. Similarly to the asymptotic result reached in equation (39), the leading-order term of the integration (41) is deduced using partial integration, namely,

$$\Psi(\rho=0,z,t) \approx \frac{-\Psi_0(D/2)}{2(\omega_0 T)^2\left((1/\gamma)\sqrt{z^2+(D/2)^2}-(D/2)\right)}\mathrm{e}^{-\mathrm{i}(\omega_0/c)(\sqrt{z^2+(D/2)^2}-ct)} \times \mathrm{e}^{\mathrm{i}(\omega_0/c)(D/2\gamma)}\left\{1+2\left(\omega_0 T-(\mathrm{i}/2cT)\left(\sqrt{z^2+(D/2)^2}-(D/2\gamma)-ct\right)\right)^2\right\} \tag{43}$$

for $z > (D/2)\sqrt{\gamma^2-1}$. According to this expression, the peak of the pulse occurs at $\sqrt{z^2+(D/2)^2}-(D/2\gamma) = ct$ and decreases as $1/z$. As $z \gg (D/2)$, the velocity of the peak of the pulse approaches that of light.

The same results are confirmed by calculating the magnitude of the pulse given in equation (41) after integrating numerically over ρ'. The results of such integration are plotted in figures 10–12. In these figures, we have chosen the radius of the axicon to equal $(D/2) = 0.05$ m. In figure 10, we have plotted the pulsed Bessel beam for $(\omega_0/c) = 4\times10^6$ m^{-1} and $cT = 0.0006$ m. The pulse is plotted at observation times $ct_0 = 0.4$, 1.2, 2.0 and 2.8 m. Figure 10 shows a distinct propagation at a velocity greater than c. The positions of the peak of the pulse at different observation points are plotted in figure 12. At the beginning, the velocity of the peak of the pulse is much larger than the speed of light. Away from the axicon, the curve in figure 12 levels up, indicating that the velocity of the pulse asymptotically approaches c as the pulse advances deep into the far-field range. In figure 11, the same calculations are repeated for $(\omega_0/c) = 1\times10^5$ m^{-1} and $cT = 0.000\,06$ m. The positions of the peaks of this pulse are identical to those associated with that illustrated in figure 10. This is confirmed by comparing the two curves in figure 12, which show that the observation times of the peaks of pulses in both cases are equal. Because of the short axial width of the latter pulse, the observability of its superluminal propagation would be more pronounced. Finally, one should note that the quantity $(z_{\max}-ct_0)$ is positive contrary to the case of the annular slit (cf figures 6 and 7). This might lead one to believe that such pulses can violate special relativity in a global sense; i.e. that we can generate a pulse that travels faster than a simultaneously generated signal travelling with velocity c. However, this is not the case because the phase factor employed

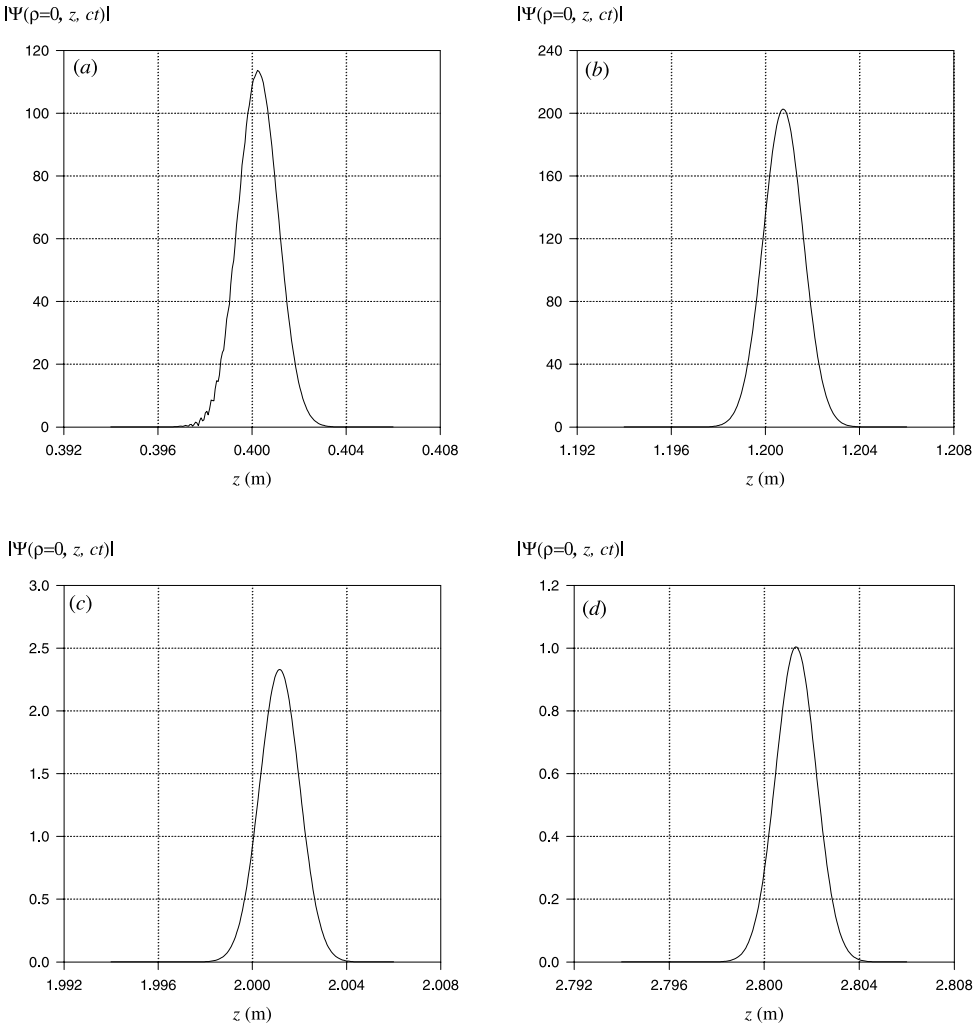

Figure 10. Axial time envelope of a pulsed Bessel beam generated by a refractive axicon having $(D/2) = 0.05$ m, $\gamma = 28$, $(\omega_0/c) = 4 \times 10^6$ m^{-1} and $cT = 0.0006$ m. The pulse is plotted at observation times: (*a*) $ct_0 = 0.4$ m; (*b*) $ct_0 = 1.2$ m; (*c*) $ct_0 = 2.0$ m; and (*d*) $ct_0 = 2.8$ m.

in equations (35) and (40) to model the action of the axicon is an approximation. Such an approximation neglects the effect of the thickness of the axicon [26]. Along the propagation axis, the difference in the optical path length representing the passage through the axicon equals $(D/2)(n-1)\tan\xi = (D/2\gamma)$. For the parameter values adopted in this study, the passage through the axicon introduces a time delay equal to $ct_d = 1.786 \times 10^{-3}$ m. This time delay, when added to the observation times ct_0 causes the quantity $(z_{\max} - c(t_0 + t_d))$ to be negative for all positions. This means that the pulsed Bessel beam generated from an axicon will be always slower than a simultaneously generated pulse travelling at the speed of light. Consequently, the propagation of a pulsed Bessel beam does not violate special relativity in a global sense. The superluminal velocity of its peak is a local behaviour that occurs in the near-field range.

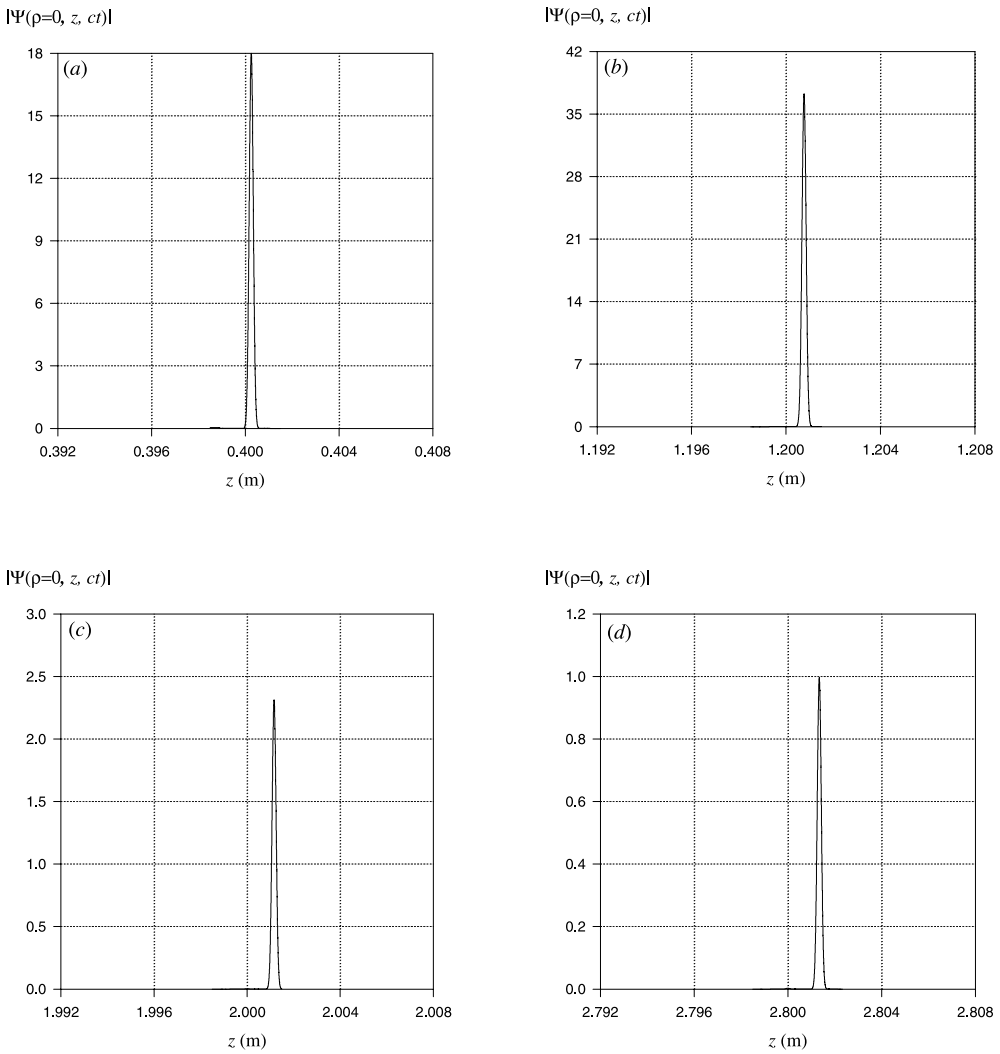

Figure 11. Same as in figure 10 but the axial time envelope of the pulsed Bessel beam is plotted for $(\omega_0/c) = 1 \times 10^5$ m^{-1} and $cT = 6 \times 10^{-5}$ m.

4.3. Pulsed Bessel beam generated by a diffractive axicon

A diffractive axicon is a holographic optical element designed for a specific frequency to produce phase differences that are linearly dependent on ρ'. In the case of a pulsed illumination of the axicon, the phase factor associated with the diffractive type is $\exp\{\mathrm{i}(\omega_0/c)(\rho'/\gamma)\}$, instead of the variable-frequency phase $\exp\{\mathrm{i}(\omega/c)(\rho'/\gamma)\}$ used for refractive axicons. Here, ω_0 is the angular frequency, for which the circular grating is designed. In the following calculations, ω_0 is the mean frequency of the Gaussian envelope used in the initial pulsed field

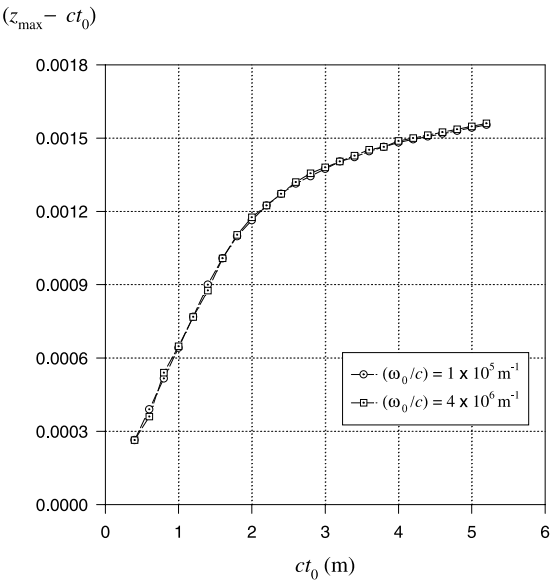

Figure 12. Positions of the peaks of the pulsed Bessel beams generated by a refractive axicon at different observation times. The positions of the peaks are plotted for the two frequencies $(\omega_0/c) = 4 \times 10^6$ m^{-1} and $(\omega_0/c) = 1 \times 10^5$ m^{-1}.

given in equation (31). Consequently, the amplitude of the on-axis field equals

$$\Psi_p(\rho = 0, z, t) = \frac{\mathrm{i}\Psi_0}{(\omega_0/c)} \int_0^{(D/2)} \mathrm{d}\rho' \, \frac{\rho'}{\sqrt{z^2 + \rho'^2}} \int_0^{\infty} \mathrm{d}(\omega/c)\,(\omega/c)^2 \big(cT/\sqrt{\pi}\big) \mathrm{e}^{-(\omega-\omega_0)^2 T^2}$$
$$\times \mathrm{e}^{+\mathrm{i}\omega t} \mathrm{e}^{-\mathrm{i}(\omega/c)\sqrt{z^2+\rho'^2}} \mathrm{e}^{\mathrm{i}(\omega_0/c)(\rho'/\gamma)}. \tag{44}$$

Integrating over (ω/c) after extending the limits from $-\infty \to +\infty$, we obtain

$$\Psi_p(\rho = 0, z, t) \cong \mathrm{i}\Psi_0 \int_0^{(D/2)} \mathrm{d}\rho' \, \frac{\rho'}{\sqrt{z^2 + \rho'^2}} \mathrm{e}^{-(\sqrt{z^2+\rho'^2} - ct)^2/4c^2T^2} \mathrm{e}^{\mathrm{i}(\omega_0/c)(\rho'/\gamma)}$$
$$\times \mathrm{e}^{-\mathrm{i}(\omega_0/c)(\sqrt{z^2+\rho'^2} - ct)} (\omega_0/c)$$
$$\times \big\{1 + 2\big(\omega_0 T - (\mathrm{i}/2cT)\big(\sqrt{z^2 + \rho'^2} - ct\big)\big)^2\big\} \big/ (\omega_0 T)^2. \tag{45}$$

The leading order of this integration can be evaluated using the stationary phase analysis applied previously to the case of monochromatic illumination. The stationary phase method leads to the following expression for the axicon-generated pulsed Bessel beam:

$$\Psi_p(\rho = 0, z, t) \approx \mathrm{i}\Psi_0 \sqrt{2\pi\gamma(\omega_0/c)}\, \mathrm{e}^{-(z(\gamma/\sqrt{\gamma^2-1}) - ct)^2/4c^2T^2} \mathrm{e}^{-\mathrm{i}(\omega_0/c)(z(\gamma/\sqrt{\gamma^2-1}) - ct)}$$
$$\times \mathrm{e}^{\mathrm{i}(\omega_0/c)(z/\sqrt{\gamma^2-1})} \mathrm{e}^{-\mathrm{i}(\pi/4)} \big(\sqrt{z}/(\gamma^2 - 1)^{3/4}\big)$$
$$\times \big\{1 + 2\big(\omega_0 T - (\mathrm{i}/2cT)(z(\gamma/\sqrt{\gamma^2 - 1}) - ct)\big)^2\big\}/2(\omega_0 T)^2 \tag{46}$$

for $0 < z < (D/2)\sqrt{\gamma^2 - 1}$. This pulse has a Gaussian axial width and a centre moving at a subluminal velocity $v_p = \big(\sqrt{\gamma^2 - 1}/\gamma\big)c$. Similarly to the asymptotic result reached in equation (43), the leading-order term of the integration (45) is deduced using partial integration,

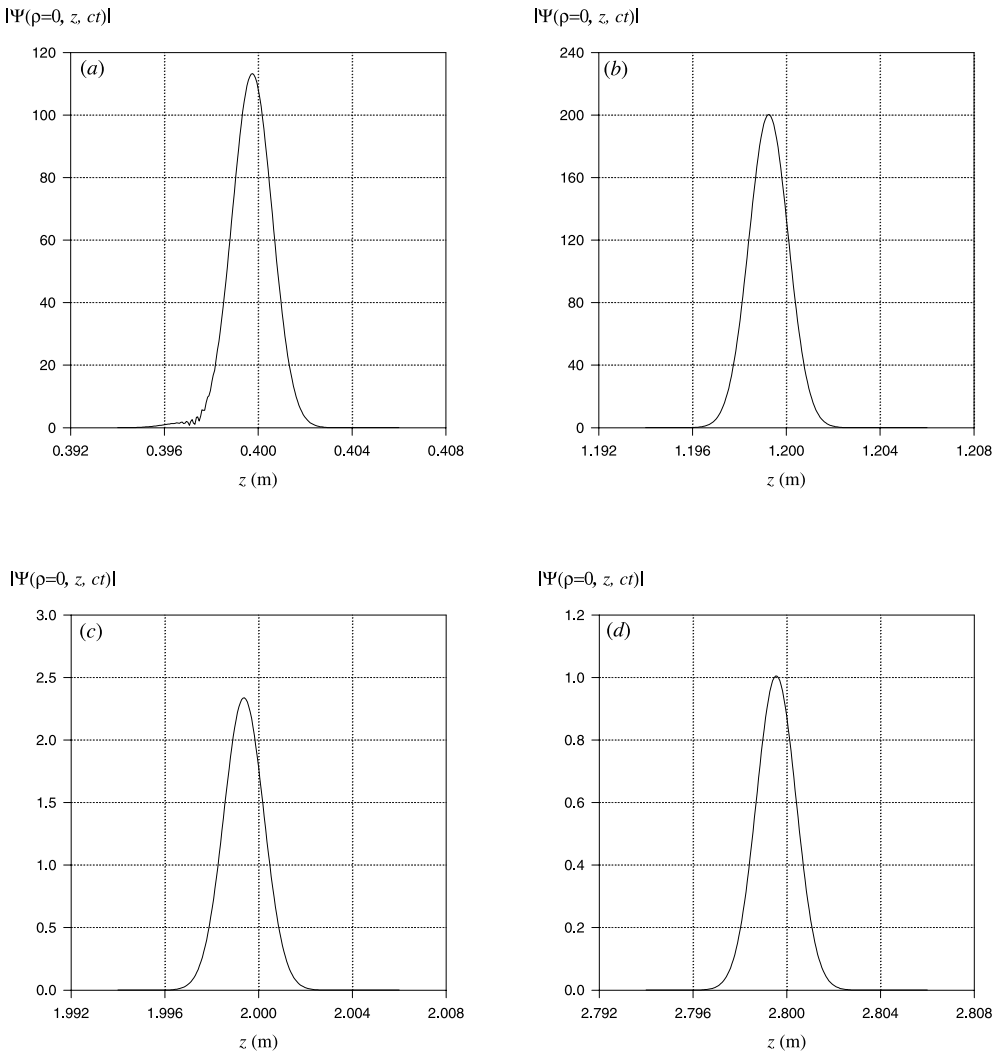

Figure 13. Axial time envelope of a pulsed Bessel beam generated by a diffractive axicon having $(D/2) = 0.05$ m, $\gamma = 28$, $(\omega_0/c) = 4 \times 10^6$ m^{-1} and $cT = 0.0006$ m. The pulse is plotted at observation times: (*a*) $ct_0 = 0.4$ m; (*b*) $ct_0 = 1.2$ m; (*c*) $ct_0 = 2.0$ m; and (*d*) $ct_0 = 2.8$ m.

namely,

$$\Psi(\rho = 0, z, t) \approx \frac{-\Psi_0(D/2)}{2(\omega_0 T)^2\big((1/\gamma)\sqrt{z^2 + (D/2)^2} - (D/2)\big)} \mathrm{e}^{-\mathrm{i}(\omega_0/c)(\sqrt{z^2+(D/2)^2}-ct)} \times \mathrm{e}^{\mathrm{i}(\omega_0/c)(D/2\gamma)} \Big\{1 + 2\big(\omega_0 T - (\mathrm{i}/2cT)\big(\sqrt{z^2 + (D/2)^2} - (D/2\gamma) - ct\big)\big)^2\Big\} \tag{47}$$

for $z > (D/2)\sqrt{\gamma^2 - 1}$. According to this expression, the peak of the pulse occurs at $\sqrt{z^2 + (D/2)^2} - (D/2\gamma) = ct$. This means that the velocity of the peak becomes superluminal and approaches c as the distance z is increased. We calculate the amplitude of the pulse given in equation (45) by numerically integrating over ρ'. The results of such an integration are plotted in figures 13–15. The size of the axicon is chosen to equal $(D/2) = 0.05$ m. In figure 13, the

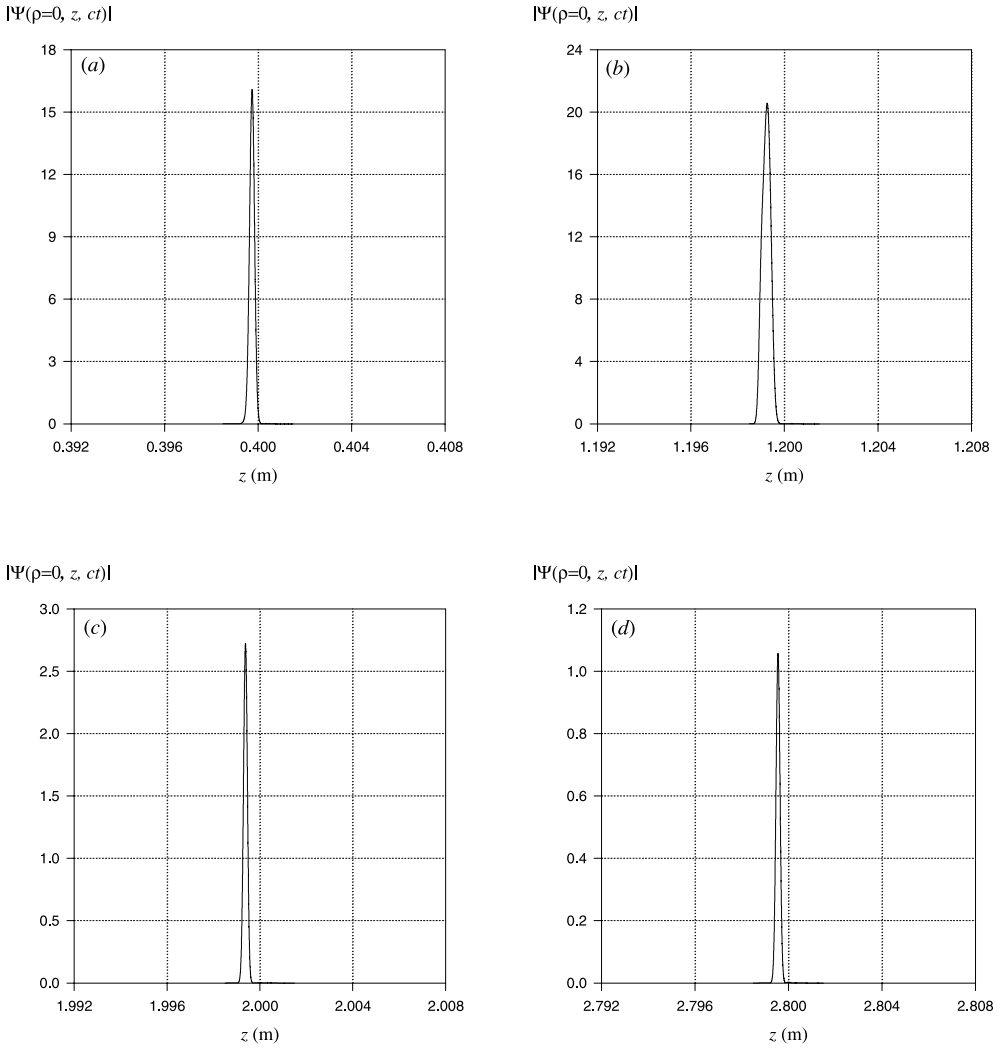

Figure 14. Same as in figure 13 but the axial time envelope of the pulsed Bessel beam is plotted for $(\omega_0/c) = 1 \times 10^5$ m^{-1} and $cT = 6 \times 10^{-5}$ m.

pulsed Bessel beam is plotted for $(\omega_0/c) = 4 \times 10^6$ m^{-1} and $cT = 0.0006$ m and observation times equal to $ct_0 = 0.4$, 1.2, 2.0 and 2.8 m. Unlike the case of a refractive axicon, the pulse starts by travelling at a subluminal speed in the near-field range. Once it crosses over the near-to-far field limit, it acquires a superluminal velocity that asymptotically approaches c as the pulse advances deep into the far-field range. This picture is confirmed in figure 15, where the positions of the peak of the pulse are plotted for different observation times. In this figure, intervals having negative (positive) slopes correspond to subluminal (superluminal) velocities. The same calculations are repeated for $(\omega_0/c) = 1 \times 10^5$ m^{-1} and $cT = 0.000\,06$ m and the results are shown in figures 14 and 15. Similarly to the refractive axicon, the peaks of the shorter pulse are observed at the same times as those of the longer one (cf figure 15). One should also note that the shorter pulse (having a larger bandwidth) undergoes more dispersion in the near field as can be seen from figure 14(*b*).

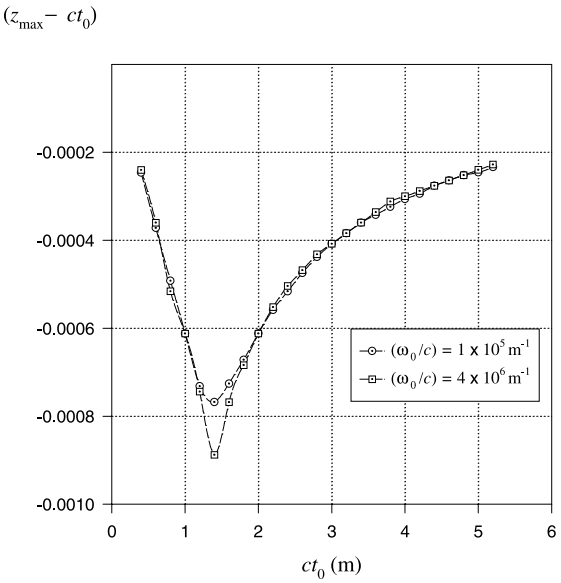

Figure 15. Positions of the peaks of the pulsed Bessel beams generated by a diffractive axicon at different observation times. The positions of the peaks are plotted for the two frequencies $(\omega_0/c) = 4 \times 10^6$ m^{-1} and $(\omega_0/c) = 1 \times 10^5$ m^{-1}.

5. Concluding remarks

We have investigated the behaviour of pulsed Bessel beams generated using various excitation schemes. Special attention has been given to determining the velocity of the peak of the propagating pulses. The field generated from an aperture has been calculated using the Rayleigh–Sommerfeld integral. Other approximate formulae, such as the Fresnel or the Fraunhofer integrals, have not been used because of their limited validity for specific distances from the generating aperture. In contradistinction, the Rayleigh–Sommerfeld formula yields expressions that are valid continuously both in the near- and far-field ranges. The current study has shown that the velocity of the peak of pulsed Bessel beam depends on the spatio-temporal profile of the excitation field. Pulsed Bessel beams generated from circular arrays can thus travel at either subluminal (subsonic) or superluminal (supersonic) speeds. A source excited using a Bessel beam that is time-limited uniformly over the whole aperture plane produces subluminal pulsed Bessel beams. Numerical calculations undertaken in subsection 2.2 depict the subluminal pulse propagation in agreement with the experimental results reported in [8]. Generating a pulse having a superluminally propagating peak requires that the various elements of the circular array should be driven at different times using independent excitation sequences. This procedure produces X-shaped LW pulses analogous to the X-wave [2] and the Bessel X-pulse [3–5]. The same effect may be achieved by using uniform excitation followed by appropriate time delays at different parts of the aperture. Such delays can be achieved in practical situations by employing uniform illumination of an annular slit [17–19, 23] or an axicon [23, 26–33].

For the case of uniform illumination of the annular slit, we have shown that the pulse is generated at a delayed time. This is the case because a finite time is needed for waves coming from the annular slit to interfere on the axis of propagation. In the near-field range, the peak travels at a superluminal velocity. As it travels deeper into the far-field range, the velocity of the peak of the pulse approaches asymptotically the speed of light. The individual spectral plane wave components travel at the speed of light, while the peak resulting from their interference propagates with superluminal velocity. For a pulsed Bessel beam generated using

a refractive axicon, it has been shown that in the near-field range (i.e. $z < (D/2)\sqrt{\gamma^2 - 1}$) the peak of the pulse travels at superluminal velocities and the amplitude of the peak increases as $\sqrt{z}$. The analysis employed in this investigation, shows that the peak of the pulse travels at a superluminal velocity even for $z > (D/2)\sqrt{\gamma^2 - 1}$ as illustrated in figures 10–12. The velocity of the peak of the pulse, however, approaches c as the pulse travels deeper into the far-field range. It has also been shown that for a diffractive axicon the velocity of the peak of the generated pulse is initially subluminal. For $z > (D/2)\sqrt{\gamma^2 - 1}$, the pulse becomes superluminal and its velocity approaches asymptotically the speed of light at larger distances.

All numerical results produced in this work indicate that the superluminal velocities acquired by X-shaped pulses generated by a circular array, an annular slit or an axicon should be detectable especially when ultrashort pulses are used. The peak of a generated pulse travels at a superluminal velocity for a finite distance L; beyond this distance the speed of the pulse approaches asymptotically that of light. Although the examples used for numerical evaluations have L values of a few metres, one can design sources that can produce superluminal pulses over longer ranges. All generation schemes, however, share the common feature of undergoing a 'delayed generation' of the pulses followed by superluminal 'catching up'. At distance L, a superluminal pulse would catch up with a simultaneously generated pulse that has been launched without any 'delayed generation' and is travelling at the speed of light. This means that, globally, pulsed Bessel beams would travel at speeds less than that of light. Therefore, the generation of such pulses does not contradict the theory of special relativity. However, such pulses travel at superluminal velocities between any two points within the range L. The observed superluminality is thus a local phenomenon achievable only over a finite distance from the source and is particularly noticeable when ultrashort pulses are used. The contingent superluminal local signalling using X-shaped pulses and possible effects on relativistic causality are discussed in [65].

Acknowledgments

The first author wishes to thank Professor Erasmo Recami, of the University of Bergamo, for the stimulating discussions about the superluminality of X-waves. He acknowledges that these discussions were the impetus for this work. The first author would also like to express his gratitude to Dr Flavio Fontana, of Pirelli Cavi e Sistemi (Milano), for his hospitality and the interesting discussion concerning optical methods for generating X-waves.

References

[1] Lu J Y and Greenleaf J F 1992 Nondiffracting X waves—exact solutions to free space scalar wave equation and their finite aperture realization *IEEE Trans. Ultrason. Ferroelec. Freq. Contr.* **39** 19–31

[2] Lu J Y and Greenleaf J F 1992 Experimental verification of nondiffracting X waves *IEEE Trans. Ultrason. Ferroelec. Freq. Contr.* **39** 441–6

[3] Saari P and Sõnajalg H 1997 Pulsed Bessel beams *Laser Phys.* **7** 32–9

[4] Saari P and Reivelt K 1997 Evidence of X-shaped propagation-invariant localized light waves *Phys. Rev. Lett.* **79** 4135–8

[5] Sõnajalg H, Rastep M and Saari P 1997 Demonstration of the Bessel-X pulse propagating with strong lateral and longitudinal localization in a dispersive medium *Opt. Lett.* **22** 310–2

[6] Besieris I M, Abdel-Rahman M, Shaarawi A M and Chatzipetros A A 1998 Two fundamental representations of localized pulse solutions of the scalar wave equation *Progr. Electromagn. Res.* **19** 1–48

[7] Recami E 1998 On localized X-shaped superluminal solutions to Maxwell's equations *Physica* A **252** 586–610

[8] Rodriguez W A Jr and Lu J Y 1997 On the existence of undistorted progressive waves (UPWs) of arbitrary speeds $0 \leqslant v < \infty$ in nature *Found. Phys.* **27** 435

[9] Barashenkov V S and Rodriguez W A Jr 1998 Launching of non-dispersive sub- and superluminal beams *Nuovo Cimento* B **113** 329–38
[10] Capelas de Oliviera E and Rodriguez W A Jr 1998 Superluminal electromagnetic waves in free-space *Ann. Phys., Lpz.* **7** 654–9
[11] Donnelly R, Power D, Templeman G and Whalen A 1994 Graphic simulation of superluminal acoustic localized wave pulses *IEEE Trans. Ultrason. Ferroelec. Freq. Contr.* **41** 7–12
[12] Fagerholm J, Friberg A T, Huttunen J, Morgan D P and Salomaa M M 1996 Angular-spectrum representation of nondiffracting X waves *Phys. Rev.* E **54** 4347–52
[13] Friberg A T, Fagerholm J and Salomaa M M 1997 Space-frequency analysis of nondiffracting pulses *Opt. Commun.* **136** 207–12
[14] Ziolkowski R W, Besieris I M and Shaarawi A M 1993 Aperture realizations of the exact solutions to homogeneous-wave equations *J. Opt. Soc. Am.* A **10** 75–87
[15] Chatzipetros A A, Shaarawi A M, Besieris I M and Abdel-Rahman M A 1998 Aperture synthesis of time-limited X-waves and analysis of their propagation characteristics *J. Acoust. Soc. Am.* **103** 2287–95
[16] Shaarawi A M 1997 Comparison of two localized wavefields generated from dynamic apertures *J. Opt. Soc. Am.* A **14** 1804–16
[17] Durnin J 1987 Exact solutions for nondiffracting beams. I. The scalar theory *J. Opt. Soc. Am.* A **4** 651–4
[18] Durnin J, Miceli J J Jr and Eberly J H 1987 Diffraction free beams *Phys. Rev. Lett.* **58** 1499–501
[19] Durnin J, Miceli J J Jr and Eberly J H 1988 Comparison of Bessel and Gaussian beams *Opt. Lett.* **13** 79–80
[20] Gori F, Guattari G and Padovani C 1987 Bessel–Gauss beams *Opt. Commun.* **64** 491–5
[21] Vicari I 1989 Truncation of nondiffracting beams *Opt. Commun.* **70** 263–6
[22] Overfelt P L and Kenney C S 1991 Comparison of the propagation characteristics of Bessel, Bessel–Gauss and Gaussian beams diffracted by a circular aperture *J. Opt. Soc. Am.* **8** 732–45
[23] Indebtouw G 1989 Nondiffracting optical beams: some remarks on their analysis and synthesis *J. Opt. Soc. Am.* A **6** 150–2
[24] Cox A J and Dibble D C 1992 Nondiffracting beams from a spatially filtered Fabry–Perot resonator *J. Opt. Soc. Am.* A **9** 282–6
[25] Horvath Z L, Erdelyi M, Szabo G, Bor Zs, Tittel F K and Cavallaro J R 1997 Generation of nearly nondiffracting Bessel beams with a Fabry–Perot interferometer *J. Opt. Soc. Am.* A **14** 3009–13
[26] Herman R M and Wiggins A T 1991 Production and uses of diffractionless beams *J. Opt. Soc. Am.* A **8** 932–42
[27] Armito R, Saloma C, Tanaka T and Kawata S 1992 Imaging properties of axicons in a scanning optical system *Appl. Opt.* **31** 6653–7
[28] Cox A J and Dibble D C 1991 Holographic reproduction of a diffraction-free beam *Appl. Opt.* **30** 1330–2
[29] Niggel L, Lanzl T and Maier M 1997 Properties of Bessel beams generated by periodic grating of circular symmetry *J. Opt. Soc. Am.* A **14** 27–33
[30] Vassara A, Turunnen J and Friberg A T 1989 Realization of general nondiffracting beams with computer-generated holograms *J. Opt. Soc. Am.* A **6** 1748–54
[31] Turnen J, Vasara A and Friberg A T 1988 Holographic generation of diffraction-free beams *Appl. Opt.* **27** 3959–62
[32] Vahimaa P, Kettunen V, Kuittinen M, Turunen J and Friberg A T 1997 Electromagnetic analysis of nonparaxial Bessel beams generated by diffractive axicons *J. Opt. Soc. Am.* A **14** 1817–24
[33] Koronkevich V P, Mikhaltsova I A, Churin E G and Yurlov Y I 1995 Lensacon *Appl. Opt.* **34** 5761–72
[34] Hsu D K, Margetan F J and Thompson D O 1989 Bessel beam ultrasonic transducer: Fabrication method and experimental results *Appl. Phys. Lett.* **55** 2066–8
[35] Lu J Y and Greenleaf J F 1990 Ultrasonic nondiffracting transducer for medical imaging *IEEE Trans. Ultrason. Ferroelec. Freq. Contr.* **37** 438–47
[36] Lu J Y and Greenleaf J F 1992 Diffraction-limited beams and their applications for ultrasonic imaging and tissue characterization *Proc. SPIE* **1733** 92–119
[37] Lu J Y, Zou H and Greenleaf J F 1994 Biomedical beam forming *Ultrasound Med. Biol.* **20** 403–28
[38] Lu J Y, Zou H and Greenleaf J F 1995 A new approach to obtain limited diffraction beams *IEEE Trans. Ultrason. Ferroelec. Freq. Contr.* **42** 850–3
[39] Lu J Y 1995 Bowtie limited diffraction beams for low-sidelobe and large depth of field imaging *IEEE Trans. Ultrason. Ferroelec. Freq. Contr.* **42** 1050–63
[40] Lu J Y, Fatemi M and Greenleaf J F 1996 Pulsed-echo imaging with X wave *Acoustic Imaging* vol 22, ed P Tortoli and L Masotti pp 191–6
[41] Lu J Y, Xu X L and Greenleaf J F 1995 Application of Bessel beam for Doppler velocity estimation *IEEE Trans. Ultrason. Ferroelec. Freq. Contr.* **42** 649–62
[42] Brittingham 1983 Focus wave modes in homogeneous Maxwell equations: Transverse electric mode *J. Appl.*

Phys. **54** 1179–89
[43] Ziolkowski R W 1985 Exact solutions of the wave equation with complex source locations *J. Math. Phys.* **26** 861–3
[44] Ziolkowski R W, Lewis D K and Cook B D 1989 Experimental verification of the localized wave transmission effect *Phys. Rev. Lett.* **62** 147–50
[45] Ziolkowski R W and Lewis D K 1990 Verification of the localized wave transmission effect *J. Appl. Phys.* **68** 6083–6
[46] Ziolkowski R W 1991 Localized wave physics and engineering *Phys. Rev.* A **44** 3960–84
[47] Ziolkowski R W 1989 Localized transmission of electromagnetic energy *Phys. Rev.* A **39** 2005–33
[48] Besieris I M, Shaarawi A M and Ziolkowski R W 1989 A bidirectional traveling plane wave representation of exact solutions of the scalar wave equation *J. Math. Phys.* **30** 1254–69
[49] Donnelly R and Ziolkowski R 1993 Designing localized waves *Proc. R. Soc.* A **440** 541–65
[50] Ziolkowski R W, Besieris I M and Shaarawi A M 1991 Localized wave representations of acoustic and electromagnetic radiation *Proc. IEEE* **79** 1371–8
[51] Shaarawi A M, Besieris I M, Ziolkowski R W and Sedky S M 1995 Generation of approximate focus wave mode pulses from wide-band dynamic Gaussian aperture *J. Opt. Soc. Am.* A **12** 1954–64
[52] Shaarawi A M, Sedky S M, Ziolkowski R W and Taiel F M 1996 Effect of the switching pattern of the illumination of dynamic apertures on the ranges of the generated waves *J. Opt. Soc. Am.* A **13** 1712–8
[53] Sedky S M, Shaarawi A M, Taiel F M and Besieris I M 1996 On the diffraction length of localized waves generated by dynamic apertures *J. Opt. Soc. Am.* A **13** 1719–27
[54] Shaarawi A M, Sedky S M, Ziolkowski R W and Besieris I M 1996 The spatial distribution of the illumination of dynamic apertures and its effect on the decay rate of the radiated localized pulses *J. Phys. A: Math. Gen.* **29** 5157–79
[55] Shaarawi A M, Ziolkowski R W and Besieris I M 1995 On the evanescent fields and the causality of the focus wave modes *J. Math. Phys.* **36** 5565–87
[56] Mugnai D, Ranfagni A and Ruggeri R 2000 Observation of superluminal behaviors in wave propagation *Phys. Rev. Lett.* **84** 4830–3
[57] Overfelt P L 1991 Bessel–Gauss pulses *Phys. Rev.* A **44** 3941–7
[58] Goodman J W 1968 *Introduction to Fourier Optics* (New York: McGraw-Hill)
[59] Abramovitz M and Stegun I A 1972 *Handbook of Mathematical functions* (New York: Dover)
[60] Satyapal S and Stepanishen P 1993 Space/time characteristics of localized transient fields from planar axisymmetric sources *J. Acoust. Soc. Am.* **93** 821–35
[61] Hafizi B and Sprangle P 1991 Diffraction effects in directed radiation beams *J. Opt. Soc. Am.* A **8** 705–17
[62] Blejer D J, Whittmann R C and Yaghijan A D 1993 On axis fields from circular uniform surface current *Proc. Int. Conf. on Ultrawideband Short Pulse Electromagnetics* ed H Bertoni, L Carin and L B Felsen (New York: Plenum)
[63] Gradshteyn I S and Ryzhik I M 1965 *Tables of Integrals, Series and Products* (New York: Academic)
[64] Bender C M and Orszag S A 1978 *Advanced Mathematical Methods for Scientists and Engineers* (New York: McGraw-Hill)
[65] Shaarawi A M and Besieris I M 2000 Relativistic causality and superluminal signalling using X-shaped localized waves *J. Phys. A: Math. Gen.* **33** 7255–63 (following paper)